

Coastal erosion processes in tidal channel Oostgat



2014

John Damen

Coastal erosion processes in tidal channel Oostgat

Master thesis - Final report

09-10-2014

John Damen

Graduation committee

Prof. Dr. S.J.M.H. Hulscher (University of Twente)

Dr. Ir. P.C. Roos (University of Twente)

Dr. Ir. J.J. van der Werf (Deltares/University of Twente)

Dr. Ir. E.P.L. Elias (Deltares)

cover photo: <https://beeldbank.rws.nl>, Rijkswaterstaat / Joop van Houdt

Preface

This report is the result of my master thesis project at Deltares (department ZKS) in Delft. It is the final stage of my master Water Engineering and Management at Twente University. It has been an educational experience to do in depth research on such an interesting topic. It has shown me how interesting research can be, which is the main cause I am looking forward to starting with my PhD at Twente University after this thesis.

I would like to thank my daily supervisor Jebbe van der Werf for the discussions and input during the process, which were very useful. Also a word of thanks to all members of my graduation committee for the involvement and valuable feedback during the process.

Next, I would like to thank Deltares for offering their facilities during my research. The ability to use the existing Delft3D-NeVla model and calculation cluster have been important to the success of my thesis. A special thanks to all the other students at Deltares for the discussions on the difficult topics and for making the master thesis period a lot of fun as well.

Finally, I would like to thank Marjan for being my inspiration.

John Damen

Delft, Oktober 2014

Summary

The coastward channel slope of tidal channel Oostgat along the coast of Walcheren (NL) migrates in landward direction by 0.2m per year between Westkapelle and Zoutelande (Tonnon and Van der Werf, 2014). In addition to annual beach nourishments of 0.2 million m³ channel slope nourishments have been applied in 2005 and 2008, with a total volume of 8.5 million m³. These measures prove effective to maintain the current coastline position as is required by the Dutch coastal policy. However, the processes responsible for the erosion are not well known. The aim of this study is to increase our understanding of the lateral migration behaviour of the tidal channel Oostgat.

To analyse sediment transports in the Oostgat, a 2DV Delft3D model has been created for the ebb-tidal delta of Scheldt estuary. Model results showed good similarity to the more calibrated model Delft3D-NeVla which includes the entire Scheldt estuary on a coarser grid.

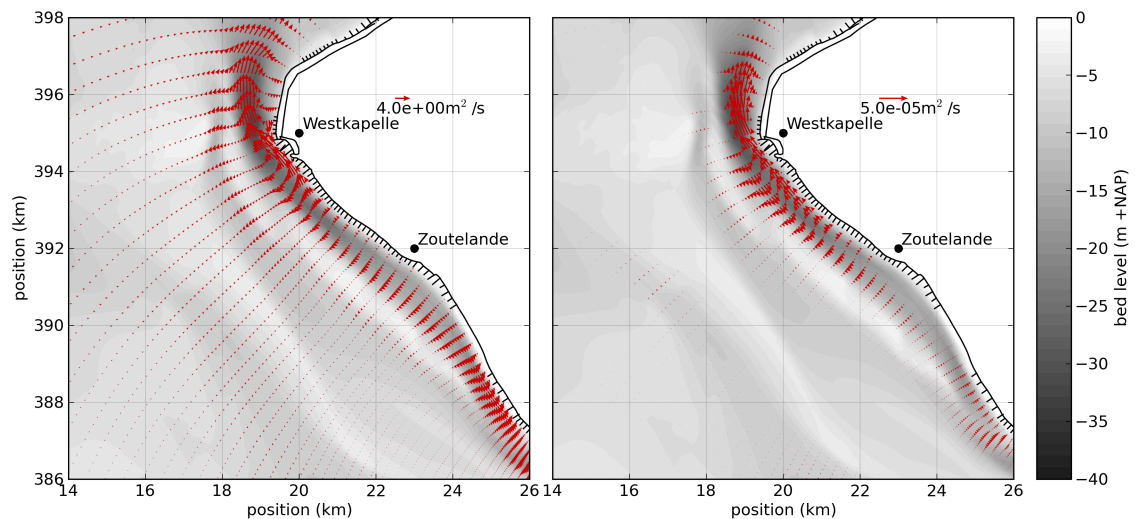


Figure 1: Net discharge (l) and residual transport (r) for a representative tidal cycle in tidal channel Oostgat

The model results show a divergence in residual sediment transports along the coastward side of the tidal channel (Figure 1) which results in erosion along the channel slope. A comparison of the influence on the coastal erosion by tide, waves and wind indicates the tide as the dominant forcing mechanism.

A shift of the flood velocities towards the outer bend near Westkapelle causes flood dominance at the seaward side of the channel with flood directed net transports. This effect can be explained by the inertia of the flow as it passes the bend in the channel. The shift of the flood velocities also causes ebb dominance at the inner bend with ebb directed net transports. A further shift of the ebb velocities towards the inner bend was also found, but could not be explained in this study. Possible causes are the contraction of the flow at the bend and a large water level gradient between the Oostgat and the area to the northeast which forces the flow along the coast. These effects should be investigated further. The results of this study increased the knowledge of the channel slope erosion processes in the Oostgat and indicated the processes that are required for the accurate modelling of sediment transport patterns in the tidal channel. This knowledge can be used to implement more efficient measures aimed at the cause of the erosion.

Contents

1	Introduction	1
1.1	Relevance of this study	2
1.2	Objective and research questions	2
1.3	Methodology	2
1.4	Outline of the report	4
2	Study area	5
2.1	Tide	5
2.2	Wind	5
2.3	Waves	6
2.4	Historical development	7
2.5	Measures	8
2.5.1	Structures	8
2.5.2	Nourishments	8
2.6	Existing descriptions of sediment transport mechanisms in tidal channel Oostgat	9
2.6.1	Transport paths derived from sand waves	9
2.6.2	Circulation cell around ‘Bankje van Zoutelande’	10
2.6.3	Increased discharge	10
3	Erosion mechanisms	11
3.1	Lateral sand supply	11
3.2	Divergence of flows in the channel behind the banks	12
3.3	Increased discharge	12
4	Model setup	13
4.1	Delft3D-NeVla	13
4.2	Grid design	14
4.3	Reduction of simulation time	14
4.3.1	Representative morphological tide	14
4.3.2	Representative wave climate	15
4.3.3	Timestep and calculation time	15
4.4	Additional model settings	16
5	Model results	17
5.1	Model cases	17
5.1.1	Tide, waves and wind (C1)	17
5.1.2	Tide (C2)	18
5.1.3	Tide and waves (C3)	21
5.1.4	Tide and wind (C4)	23
5.2	Effect of tide, waves and wind on erosion at the channel slope	25
6	Conceptual model	27
6.1	Channel discharge comparison 1973-2011	27
6.2	Sediment flux across ‘Bankje van Zoutelande’	28
6.3	Decomposition of velocities	29
6.4	Dominance of tidal flows	31
6.5	Conclusion	33

7 Discussion	35
8 Conclusion	37
9 Recommendations	39
10 References	41
A What are the assumptions and equations Delft3D uses?	43
A.1 Grid	43
A.1.1 Horizontal staggered grid	43
A.1.2 Vertical σ -grid	43
A.2 Hydrodynamic equations	44
A.3 Sediment transport	45
A.4 Existing model	45
B Representative morphological tide	47
C Representative wave climate	53
C.1 Approach	53
C.2 Results	55
D Grid design	57
D.1 Area of interest	58
D.2 Approach	58
D.3 Grid quality	59
D.4 Comparison of model results	61
E Derivation of velocity driven transport components	63

1 Introduction

The largest part of the Dutch coastline has the natural tendency to erode. Since 1990 the coast is maintained at the same position. This is achieved with nourishments of sand to compensate for the erosion where possible and solid structures where required. The Delta coast (southern part of the Dutch coastline), of which the tidal channel Oostgat is a part, has a perceived annual sediment deficit of about 9 Mm³ despite 3 Mm³ of annual beach nourishments (Cleveringa, 2008).

The tidal channel Oostgat is located just off the coast of Walcheren (south-western part of the Netherlands) and runs from Westkapelle in the north to Dishoek in the south over a distance of around 8km (Figure 1.1).

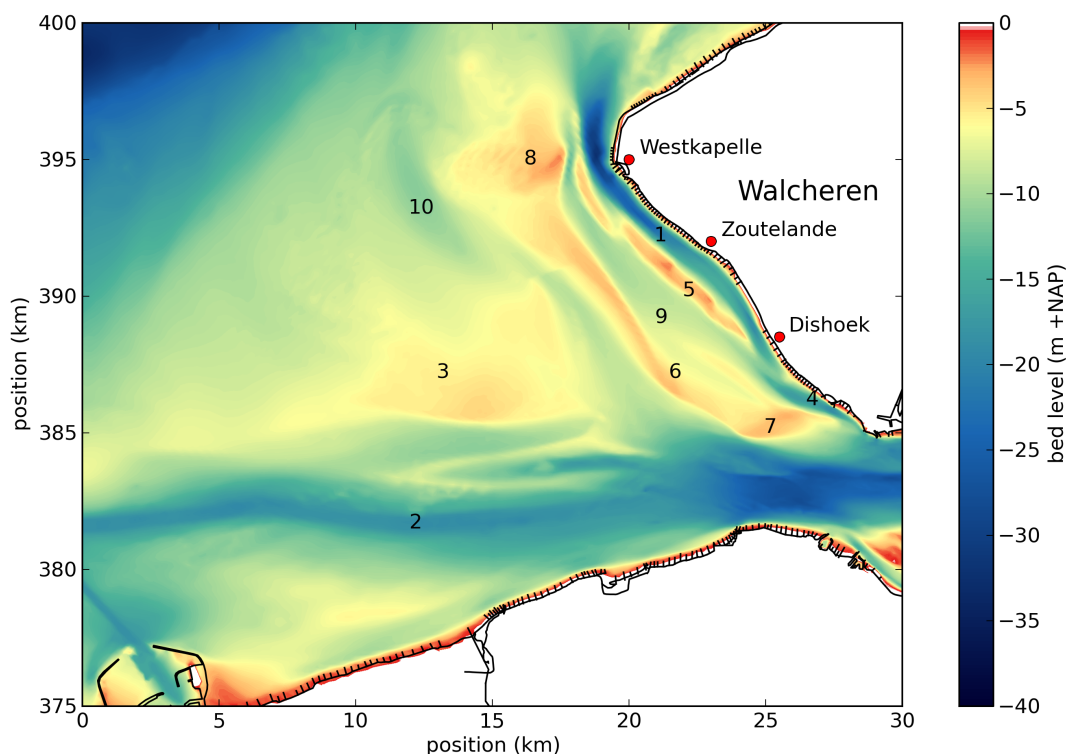


Figure 1.1: Bathymetric chart (2011) of the study area with (1) Oostgat, (2) Wielingen, (3) Vlake van Raan, (4) Sardijngemaal, (5) Bankje van Zoutelande, (6) Elleboog, (7) Nolleplaat, (8) Rassen, (9) Deurloo Oost and (10) Deurloo West

The channel shows a lateral migration of 0.2 meter per year towards the shore between Westkapelle and Zoutelande (Hordijk, 2002; Erkens, 2003; Tonnon and Van der Werf, 2014). This threatens the flood safety of Walcheren which currently allows for failure every 4000 years (Rijksoverheid Nederland, 2008). A narrowing of the beach due to the receding coastline also endangers the recreational activities along the coast.

Regular beach nourishments are applied every 2-5 years with a volume of around 0.2 Mm³ to maintain the position of the coastline (Walstra, 2005; Rijkswaterstaat, 2013; Steijn and Van der Spek, 2005; Vermaas and Bruens, 2013). The beach height can be maintained using this measure but due to the steep channel slope, sand that is meant to widen the beach in offshore direction is washed away by strong channel flows in the Oostgat.

In 2005 and 2008 sand nourishments have been applied to the channel slope between Zoutelande and Westkapelle to reduce erosion in the channel (Vermaas and Bruens, 2013). This strategy appears to be effective in maintaining the coastline position (Tonnon and Van der Werf, 2014) but the processes that are responsible for the erosion at the channel slope are not well known. This study focuses on identifying these processes to increase our understanding of the lateral migration behaviour of the tidal channel Oostgat.

1.1 Relevance of this study

Even though the position of the coastline along the Oostgat can be maintained for the nearby future with regular sand nourishments, not much is understood of the processes that cause this migration. Knowledge of the relevant processes is important to efficiently influence the migration. For sustainable future management of the coastline a better understanding of the system is essential. This knowledge can possibly be applied to similar tidal channel systems, both in the Netherlands and at other locations around the world.

Furthermore, the knowledge that is gathered in this study can be used to model the ebb-tidal delta of the Western Scheldt more accurately and more efficiently. This study evaluates the relative importance of different processes. Future modelling projects can use the gathered knowledge in their choice to include these processes in the model and decision on the level of detail that is appropriate.

1.2 Objective and research questions

The objective of this study is to identify the mechanisms responsible for the erosion at the coastward channel slope of the tidal channel Oostgat.

This objective is reached by answering the following research questions which address the different elements of the study.

1. How can the coastal erosion processes at the channel slope in tidal channel Oostgat be modelled using Delft3D?
2. What is the importance of wind, waves and tide for erosion at the coastward channel slope of the Oostgat?
3. What conceptual model can describe the coastward erosion processes?

1.3 Methodology

A numerical process-based model (Delft3D) is chosen for this study. Since the aim is to identify important processes, the ability of the model to influence these processes is important. Furthermore, the model can provide more easily available data than measurements can. A disadvantage is that model results can deviate from the real situation. However, different studies have proven the reliability of Delft3D in describing complex coastal systems (Lesser *et al.*, 2004; Elias *et al.*, 2012). Since the existing model of the Western Scheldt estuary (Delft3D-NeVla model) has already been validated based on flow velocities and discharges, only a short comparison between the existing and adjusted model is used to estimate the quality of the new model.

3D effects are not included in the model since including these effects accurately would require many σ -layers to be included in the model which would significantly increase the calculation time. This probably has an effect on the flow and transport patterns in the model. The exact influence of this effect should be determined in a later study.

The model has to be refined locally to more accurately simulate small scale processes resulting from forcing by wind, waves and tide. This refining is done by nesting a model into the coarser available model and deriving boundary conditions from the large model. A refining of the grid must result in a refining of the time step to ensure numerical stability.

A representative tide is selected from the spring-neap cycles in the Delft3D-NeVla model that best approximates the sediment transport magnitude and direction in the Oostgat. This step is required to reduce the simulation time, while maintaining accurate sediment transport patterns and magnitudes within the model.

The existing model does not incorporate waves. These can be incorporated as a set of wave conditions that each contain a single wave. Since an additional simulation is required for each of the included wave conditions, this results in long calculation times. The Opti method (Mol, 2007) is used to derive a wave climate with less conditions to approximate the transport of all conditions. This approach has also been used by Elias *et al.* (2009).

Furthermore, the model will not calculate the morphodynamics (no bed level updates). These calculations are time intensive and still have high uncertainties that are partially the result of the enlarged deviations in flow velocity since transports are related to these velocities by a power of 3 to 5. Instead, the net sediment transports for a representative tidal cycle for the situation from 2011 is used to evaluate sedimentation and erosion. Also a single sediment fraction will be included in the model. The effect of not including the sediment fractions is limited when not calculating erosion. Sediment sorting effects are not taken into account. This means that deep channels where more coarse sediment naturally accumulates at the bed (armouring) is not included. Transport rates at the bed are therefore slightly overestimated.

The relative importance of the different processes is evaluated using a process analysis. Changes are made to the representation of the tide, wind and waves in the model and the effects on the erosion of coastward channel slope will be evaluated. The net sediment volume change over the representative tidal cycle within different control volumes is used as a criterion. These control volumes are positioned on the coastward side of the channel between Westkapelle and Zoutelande.

Based on existing descriptions of the sediment transports, different mechanisms that could be responsible for the erosion are formulated. These mechanisms will be validated using the model results.

Finally, a conceptual model will be formulated that describes the processes which cause the coastward erosion of the tidal channel. This model is based on a qualitative and quantitative analysis of the flow velocities and sediment transport processes.

1.4 Outline of the report

The overall structure of the report is shown in Figure 1.2. In Chapter 2 the study area and existing knowledge of the hydrological and morphological system is described. Chapter 3 includes a description of different erosion mechanisms that might explain the coastward erosion of the Oostgat.

The setup of the Delft3D model is explained in Chapter 4. The results of this model are described in Chapter 5. Finally a conceptual model is derived from the analysis of model results which aims to explain the coastward erosion mechanisms and sediment transport patterns in the tidal channel Oostgat (Chapter 6).

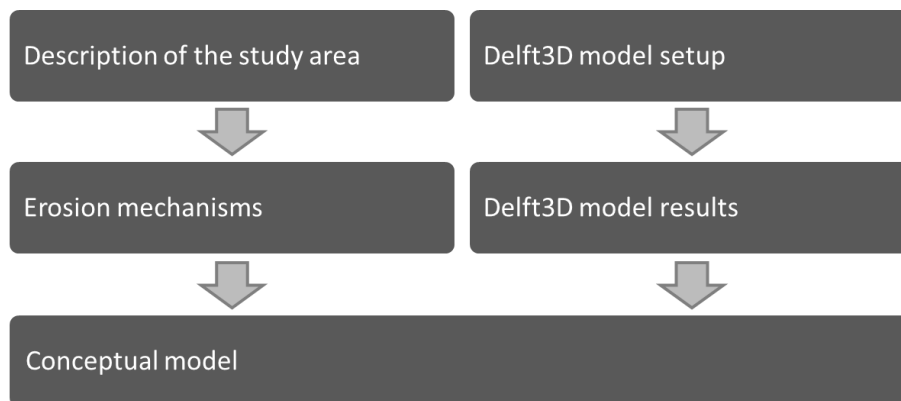


Figure 1.2: Structure of the report

The discussion of uncertainties and assumptions in the study is included in Chapter 7 followed by the conclusion in Chapter 8. Finally, recommendations for future studies and models of the Oostgat area are included in Chapter 9.

2 Study area

This study focuses on the tidal channel Oostgat and surrounding area that is relevant for the local processes at the channel. This area is located in the southeastern part of the Netherlands, off the coast of Walcheren. The channel is part of the outer delta of the Western Scheldt estuary (previously shown in Figure 1.1). The estuary is tide dominated due to the limited river discharge of an averaged $110 \text{ m}^3/\text{s}$, compared to the tidal volume of $2200 \text{ Mm}^3/\text{tide}$ at Vlissingen ($=49000 \text{ m}^3/\text{s}$) (Kuijper *et al.*, 2004). The ebb-tidal delta of the Western Scheldt has a funnel shape with two important tidal channels. The largest channel is the Wielingen which is responsible for the main part of the tidal flows to and from the Western Scheldt. The Wielingen is dredged regularly to maintain sufficient depth for large container vessels that travel to the port of Antwerp which could have further increased the tidal discharge of the channel (Tonnon and Van der Werf, 2014). The second channel is the Oostgat, which runs close to the coast of Walcheren from near Westkapelle to Dishoek towards the south, where it crosses a threshold into the Sardijngeul. To the north the channel flows into the North Sea. The Oostgat is enclosed between the coast of Walcheren to the east and the Bankje van Zoutelande to the west and has a length of around 8 km. The depth of the channel decreases from around 35m at Westkapelle to an average of 20 m at Zoutelande (Van Ormondt and De Ronde, 2009). Between the tidal channels Oostgat and Wielingen is a large shallow water area called the 'Vlakte van Raan' with low flow velocities and thus very little morphological change.

2.1 Tide

The tidal flow consists of two main aspects. The first is the northward propagating tide in the North Sea. The tidal amplitude gradually decreases as the tidal wave moves towards the north. The second is the tidal flow perpendicular to the coast which increases towards the Western Scheldt estuary. An interaction of these two flows combined with the bathymetry results in the tidal flows in the ebb-tidal delta. The incoming tide flows mainly through the Wielingen channel into the Scheldt estuary. The tidal flow in the Oostgat channel is smaller and is forced mainly by the tidal range difference between Vlissingen (3.5-4.5 m) and Westkapelle (3.0-4.0 m) (Rijksoverheid Nederland, 2008). During high tide this causes a water level gradient and a resulting flow towards Westkapelle while this reverses during low tide (Walstra, 2005).

2.2 Wind

The dominant wind direction is southwest (Steijn and Van der Spek, 2005) with an average wind velocity of around 5 m/s (Figure 2.2). Due to the orientation of this part of the coast these flows can cause a landward directed flow over the ebb-tidal delta. A less frequently occurring wind direction from the northwest causes a longshore transport. Due to the groynes present at this part of the coast the transport in this direction in the nearshore area is limited.

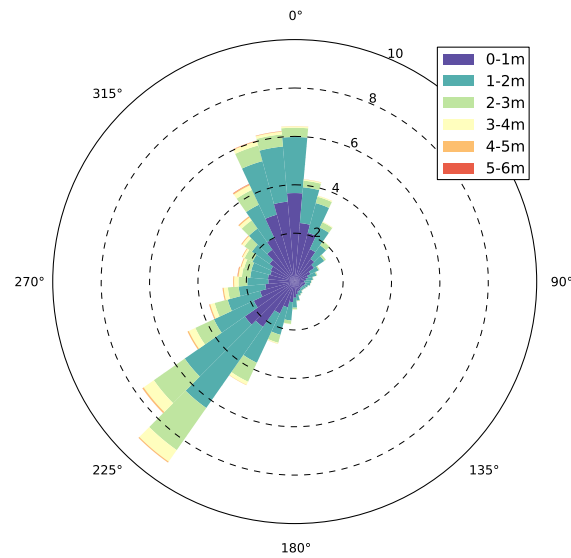


Figure 2.1: Wave directions and heights measured at Euro platform . The radial values are the percentages of occurrence

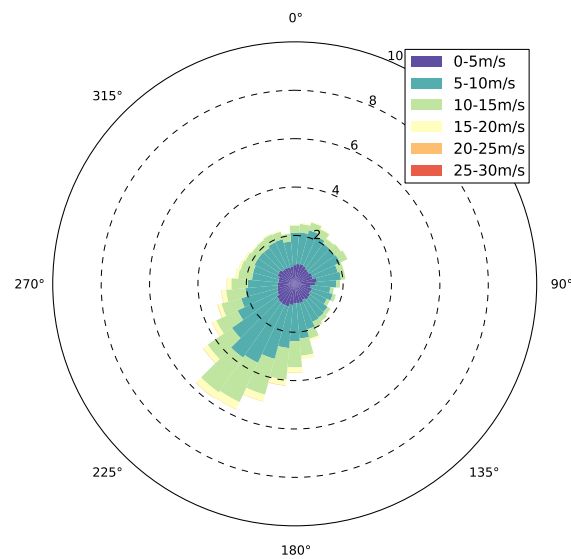


Figure 2.2: Wind directions and velocities measured at Euro platform . The radial values are the percentages of occurrence

2.3 Waves

Wave directions are mainly southwest and northwest (Figure 2.1). For most wave conditions the waves break on the beach of Walcheren but during large storms from the southwest the waves can break on the 'Bankje van Zoutelande'. The flow caused by the breaking waves results in a sediment transport to the south of around $0.2 \text{ Mm}^3/\text{year}$ in the breaker zone (Steijn and Van der Spek, 2005; Walstra, 2005). In addition, the waves stir up the sediment locally, increasing the sediment transport.

2.4 Historical development

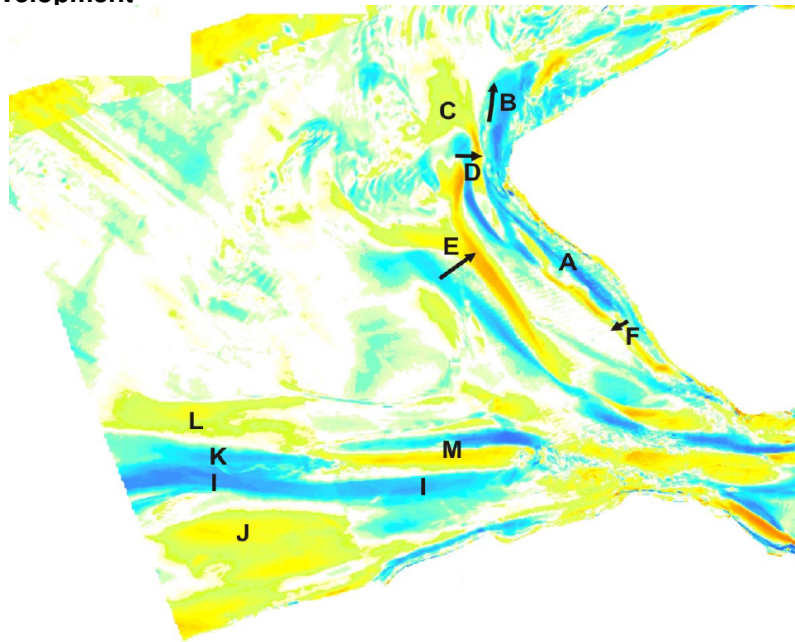


Figure 2.3: Erosion (blue) and sedimentation (red) in the Western Scheldt Ebb-tidal delta for 1964-2004 (Cleveringa, 2008)

The ebb-tidal delta of the Scheldt estuary has experienced one main change in the last two centuries. Around 1823 the outer delta consisted three main channels: Oostgat, Deurloo and Wielingen. After around 50 years the tidal channel Deurloo had lost its function as a primary tidal channel in the ebb-tidal delta. In the 19th century Deurloo split into an eastern and western part. The western part can still be found on the edge of the 'Vlakte van Raan'. The eastern part is now an extension of the Sardijngeul between the Nolleplaat-Elleboog and the 'Bankje van Zoutelande' (Steijn and Van der Spek, 2005). Two hypotheses are mentioned for this transition. The eastern part of the ebb tidal channel (Oost-Deurloo) could have rotated to the north due to a lateral sand supply. Water was therefore also flowing to the north. When halfway through the 20th century the 'Geul van de Rassen' cut into the Rassen from the south, a northern outflow for Oost-Deurloo appeared and a new system of tidal channels parallel to the coast of Walcheren was created. Another hypothesis is that dredging of the tidal channel Wielingen caused the main tidal flow to shift from the Deurloo to the Wielingen. The Deurloo and Oostgat started to function as secondary channels and channelled the flow which is forced between Vlissingen and Westkapelle. Thus changing Deurloo to a more north-south orientation.

The tidal channel Oostgat did not maintain its position over time as data over the period 1964-2004 showed (Figure 2.3). However, the morphological changes are not as large as the changes in the entire ebb-tidal delta. The channel has deepened by around 2m over the entire period (Erkens, 2003) and eroded at the coastward channel slope with an average of 0.2m per year between Westkapelle and Zoutelande (Hordijk, 2002; Erkens, 2003; Tonnon and Van der Werf, 2014) (A). Furthermore, the channel has extended towards the north (B) and sediment has been deposited at the western side of this outflow (C). The Geul van de Rassen has migrated towards the east (D). The 'Bankje van Zoutelande' has narrowed over the last 30 years with erosion at the seaward side and a steepening of the coastward slope (Figure 2.4). The bank has also increased in height, but the position has been more or less stable.

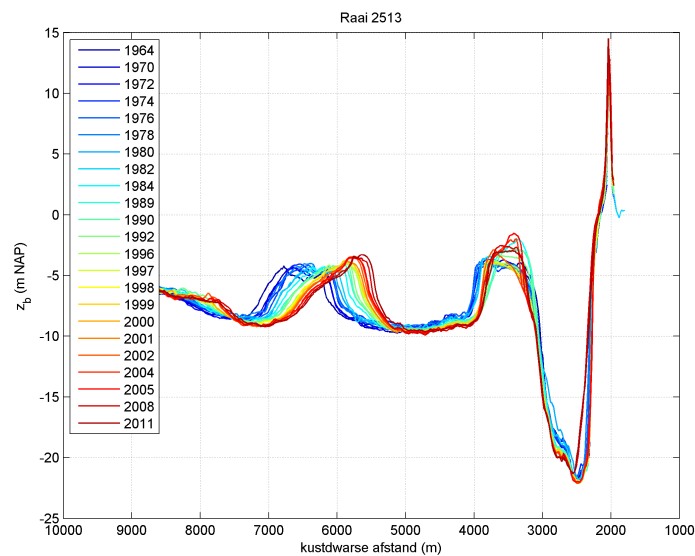


Figure 2.4: Development of transect 2513 between Westkapelle and Zoutelande (Tonnon and Van der Werf, 2014)

2.5 Measures

The natural processes have led to erosion of the coast along the Oostgat channel. To prevent the coastal erosion from threatening the integrity of the coastal defences different measures are being used. In this section the different types of measures and their implementation in the past, present and future will be described.

2.5.1 Structures

Along the coast of Walcheren there are many groynes at regular intervals which stretch out from the beach into the sea. They are meant to disrupt longshore flows and reduce erosion caused by these flows. The groynes have been built between 1856 and 1866.

At locations where a sandy coast is not feasible due to large erosion problems, sea dikes have been constructed. There are several sea dikes along the south-western coast of Walcheren. The Westkapelse Zeedijk at Westkapelle (transect 2195), the dike at Zoutelande (transect 2597-2677) and the dike at Vlissingen protect some parts of this coast.

2.5.2 Nourishments

Nourishments are interventions that use sand to maintain the coastline. Since 1990 coastal erosion is fully compensated by repeated nourishments (Steijn and Van der Spek, 2005). Nourishments exist in different types based on the location at which the sand is placed.

Beach nourishments place the sand on the beach to increase beach width and height. This measure has been applied since around 1950. The nourishment sediment was dredged at the southern part of the 'Bankje van Zoutelande' (2.2 Mm³ between 1986 and 1991) (Steijn and Van der Spek, 2005), but due to uncertainties on the impact of this dredging sand is no longer dredged at this location. The beach near the Oostgat is nourished every 2-5 years and a volume of around 0.2 Mm³/year is nourished onto the beach (intensity of 50-100m³/m per year). (Walstra, 2005; Rijkswaterstaat, 2013; Steijn and Van der Spek, 2005; Vermaas and Bruens, 2013)

Channel wall nourishments are a solution that is relevant for tidal channels that migrate in a lateral direction that is not desirable. This is the case for the Oostgat migration towards the coast that threatens coastal safety. Little experience existed for this type of measure and the effectiveness can differ per location depending on local characteristics. To increase the knowledge of this type of measure a tracer test was performed in 2001 that was evaluated by [Hordijk \(2002\)](#). After this test multiple nourishments have been applied to the channel wall. In 2005 a nourishment of 2.5 Mm³ was applied near Zoutelande (between transects 2475 and 2685) ([Van der Spek and Elias, 2013](#); [Van Ormondt and De Ronde, 2009](#); [Vermaas and Bruens, 2013](#)). This was followed by a nourishment in 2009 of 6 Mm³ near Westkapelle (between transects 2180 and 2500) ([Van der Spek and Elias, 2013](#); [Vermaas and Bruens, 2013](#)). These nourishments seem to be effective in preventing the coastward migration of the channel slope at this section of the coast according to [Tonnon and Van der Werf \(2014\)](#).

2.6 Existing descriptions of sediment transport mechanisms in tidal channel Oostgat

2.6.1 Transport paths derived from sand waves

[Erkens \(2003\)](#) described in particular the sediment transport paths in and around the tidal channel Oostgat based on the size and shape of sand waves on the bed. These were derived from multibeam data. The sediment paths that resulted from this study are displayed in [Figure 6.6](#).

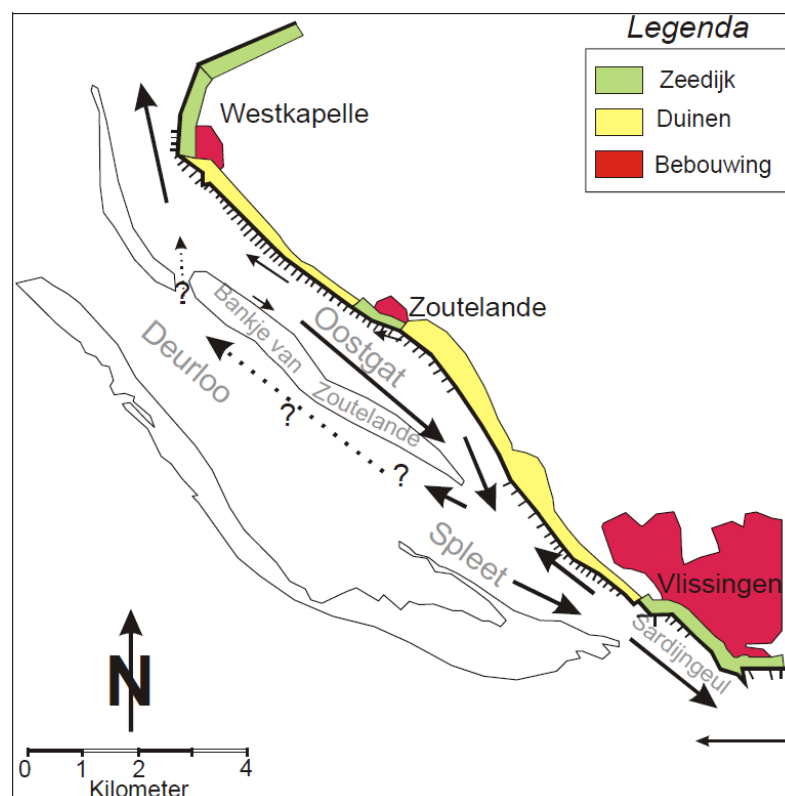


Figure 2.5: Sediment transport paths in the area of tidal channel Oostgat based on an analysis of Multibeam data ([Erkens, 2003](#)). The shape of the sand dunes on the bed was determined for many locations. The direction and scale of the sand wave shape were assumed to be strongly related to the sediment transport direction and scale.

2.6.2 Circulation cell around 'Bankje van Zoutelande'

The sediment paths as concluded by [Erkens \(2003\)](#) were used by [Steijn and Van der Spek \(2005\)](#), in combination with velocity calculations, to describe the tide averaged morphodynamic system around the Oostgat.

Under influence of the dominant flood tidal flow, sand is transported across the Nolleplaat-Elleboog and 'Bankje van Zoutelande' towards the coast. The sand that crosses the 'Bankje van Zoutelande' does not return to the coast due to the tidal flow in the Oostgat that transports it away. In the northern part sand is transported in northward direction where it becomes part of the Rassen or is possibly deposited in front of the north western coast of Walcheren. In the central part of the Oostgat the sand is transported southward, mainly along the flank of the 'Bankje van Zoutelande'. Past the threshold on the south side (Galgeput) the sand is transported back to the north by the dominant ebb tidal flow in that area (outflow Sardijngeul and transported to Oost-Deurloo). This possibly causes a circulation cell with as a consequence a semi stationary morphological state in this area.

The sand transport across the Nolleplaat-Elleboog leads to a gradual migration of this long-stretched shallow area. With the rate of migration (10-15m/year) it will take decades until the tidal channel system Sardijngeul - Oost-Deurloo - 'Geul van de Rassen' is 'squeezed' too much and the sand starts to be transported in north-south direction. There is still too little longitudinal transport capacity compared to the lateral sand influx over the Nolleplaat-Elleboog.

([Steijn and Van der Spek, 2005](#))

2.6.3 Increased discharge

Another study in literature that describes the sediment processes was done by [Hordijk \(2002\)](#). He performed a study into the effectiveness of channel slope nourishments in the tidal channel Oostgat. Data from 1969 to 2000 showed a migration of the Eastern channel slope towards the shore (erosion) and a steepening of the western channel slope caused by sedimentation of the behind the channel slope positioned 'Bankje van Zoutelande' and erosion of the western channel slope. Furthermore, the channel deepened by 2m over the period of 1969 to 2000. These results led to the following description:

A deepening of the channel combined with erosion of the channel at the shore side and a steepening of the offshore directed channel slope means an increase in the cross section and thus an increase in discharge and flow velocity through the channel. This increase in velocity results in more erosion of the channel.

([Hordijk, 2002](#))

3 Erosion mechanisms

Based on the existing knowledge of the system, mechanisms that could explain the coastward erosion in tidal channel Oostgat are formulated in this chapter. The mechanisms are explained using schematic images. The legend for the different colors is shown in Figure 3.1



Figure 3.1: Legend for colors in schematic representations of mechanisms

3.1 Lateral sand supply

The coastward directed net discharge across the banks would result in a coastward directed sediment transport, which results in a slow migration of the banks towards the coast (1: Figure 3.2a). This causes a narrowing of the channel, which increases flow velocities and sediment transports and results in erosion along the entire cross section assuming the discharge remains constant. The coastward channel slope consists of compressed clay and peat layers which reduces erosion effects on this side of the channel. The combination of the migrating banks and the resisting effects in opposite direction at the coastward channel slope result in the deepening of the channel and steepening of the channel slope (2: Figure 3.2b). The net effect of these processes is shown in Figure 3.2c. This development is consistent with the measured bathymetry development discussed in section 2.4.

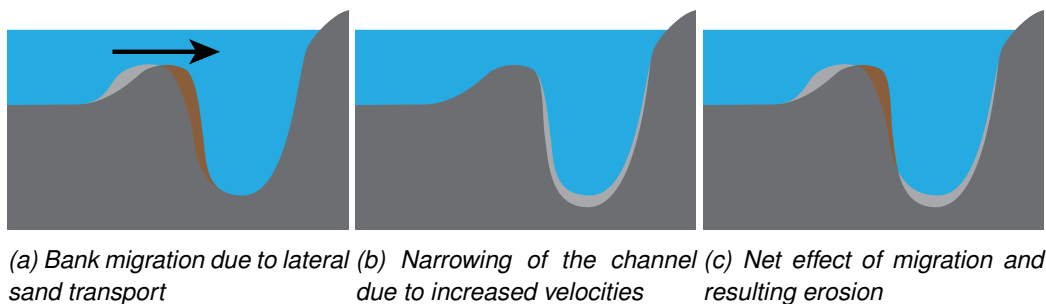


Figure 3.2: A schematic representation of migration of the banks towards the coast which results in erosion at the coastward channel slope. This erosion is reduced on the coastward slope by compressed clay layers. A constant discharge through the narrowed cross section results in erosion in other parts of the cross section.

3.2 Divergence of flows in the channel behind the banks

The net onshore discharge across the 'Bankje van Zoutelande' is discharged both to the northern and southern outflow of the channel. The inflow along the entire bank results in increasing velocities towards the outer ends of the channel and causes increasing sediment transports in those directions. This divergence in transports behind the banks causes erosion of the channel cross section.

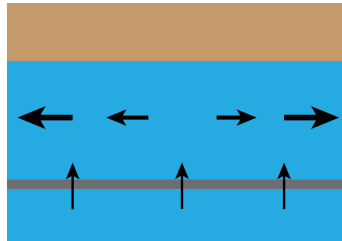


Figure 3.3: Net discharge across the banks and divergence of the flow in the channel

3.3 Increased discharge

Due to multiple possible causes, such as sea level rise and dredging in the Western Scheldt estuary, the discharge could increase. This increase in discharge should be evaluated by comparing model results for both current and historical bathymetries. Assuming there has indeed been an increase in discharge through the tidal channel Oostgat, this would cause an increase in velocities in the channel if there has been no change in the cross sectional shape. The higher flow velocities then cause more erosion of the channel until a new equilibrium has been reached between discharge and cross sectional area. An implication of this mechanism is that the erosion would reduce once a new equilibrium between discharge and cross sectional area has been reached.

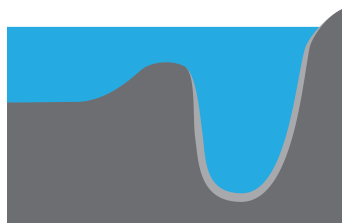


Figure 3.4: Increased channel discharge causes increased flow velocities which result in erosion of the channel cross section

4 Model setup

In this chapter the setup of the model that was used for this study is described. The model is based on an existing model called Delft3D-NeVla. Some improvements that increase model quality near tidal channel Oostgat have been made. The improvements to model quality lead to an increase of calculation time, which is then reduced by decreasing the space and time domain. The reasons for these improvements are explained as well as the steps that were taken. Finally model limitations are discussed as well as their effect on the results.

4.1 Delft3D-NeVla

The Delft3D-NeVla model has been used before in a study into the coastward migration of tidal channel Oostgat (Tonnon and Van der Werf, 2014). It is based on the NeVla-Simona model which has been calibrated for the year 2006. This calibration has been done based on astronomical tidal components and ebb/flood waterlevels for the rivers. This model has been converted to a Delft3D-model and morphological processes have been implemented. This new model has also been calibrated (based on water levels and estuary discharges). An extensive explanation of the conversion and calibration can be found in the report by Grasmeijer (2013). The model covers the Scheldt rivers, the estuary and outer delta (see Figure 4.1). The aim of the model study was to provide an accurate description of the processes within the estuary. For the present study the focus is on the outer delta and specifically the tidal channel Oostgat. This means some attributes of the model have to be changed. These changes are described in the next sections.

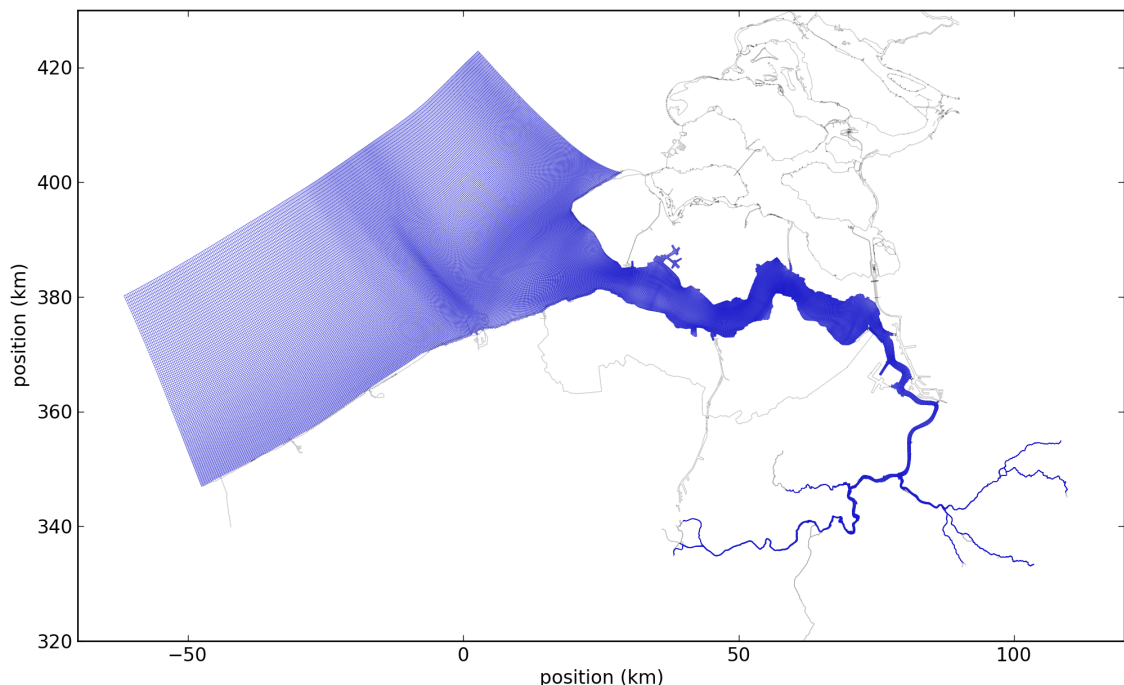


Figure 4.1: Calculation grid Delft3D-NeVla model

4.2 Grid design

The existing NeVla model has grid cells of 60x160m at the Oostgat. With a channel width of around 1km, the current resolution is too coarse for a detailed study into the processes that determine the lateral migration of the channel. A refined grid is designed that can be nested in the NeVla model (boundary conditions at the open boundaries are derived from the larger model). The process of designing the grid is explained in appendix D. The resulting grid (Figure 4.2) has a resolution of 25x25m at the Oostgat.

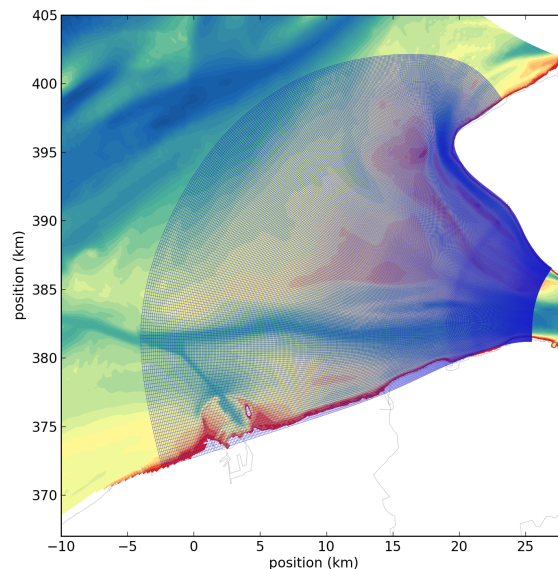


Figure 4.2: Refined calculation grid of the Western Scheldt outer delta

The refined model is neither calibrated nor validated against measured data. Instead, the NeVla model that has been calibrated and validated, is used for a quality assessment of the refined model. The comparison is done for water level, flow velocities, bed load transport and suspended sediment transport. These parameters are evaluated at three locations in and near the study area (see appendix D.4). The results show a good similarity between the models for water levels and flow velocities. Larger deviations are visible for bed load and suspended sediment transport. However, the original model has not been calibrated on these parameters, so without additional data it is not possible to contribute the differences to either further inaccuracies from reality or improvements due to the additional detail in the model.

4.3 Reduction of simulation time

The refinement of the calculation grid results in a significant increase in calculation time. Several adjustments are made to again reduce the time it takes to run the simulation. It is important to capture the representative processes in the channel to explain the erosion at the coast. The adjustments include a representative morphological tide, representative wave conditions and determining the new model timestep.

4.3.1 Representative morphological tide

The NeVla model simulated a time series of several spring-neap cycles. By reducing the length of this timeseries the simulation time can be reduced substantially. A representative subset of this timeseries is defined for further simulations. For this subset a single tidal cycle and a combination of two tidal cycles have been investigated based on the difference in net transports compared to

the spring neap cycles. A set of best options was selected by calculating the Root Mean Square of these differences. The final selection from this set is based on a qualitative comparison to account for the location and direction of the deviations in transport. A detailed description of this analysis can be found in appendix B. The selected representative tide occurs between the 11th of May 2006 at 22:30 and the 12th of May 2006 at 10:50.

4.3.2 Representative wave climate

Within the study area many different wave conditions occur. These can be of varying direction and height. The number of conditions is reduced to 9 to limit the calculation time of wave-driven transports. In a study performed by Van Rijn (2012) on a representative wave climate for the Western Scheldt, a wave time series was binned by wind velocity and direction which resulted in 54 wind conditions. Since the Western Scheldt wave-driven transports are not necessarily representative for the Oostgat the selection of representative conditions is done based on tide averaged transports inside the Oostgat using the Opti algorithm (Mol, 2007). The procedure is further explained in appendix C. The conditions that were selected from the wave climate are shown in table 4.1.

Table 4.1: Representative wave conditions

#	Weight [-]	Height (m)	Direction (°)
3	.0683	0.55	9.64
5	.2270	1.07	7.45
14	.4125	0.75	201.30
19	.0076	0.92	223.91
26	.1581	1.88	231.46
33	.0287	1.07	262.01
40	.0467	2.38	285.37
45	.0268	1.35	325.46
52	.0262	1.31	356.72

4.3.3 Timestep and calculation time

The NeVla model has a timestep of 7.5 seconds. It simulates around 3.9 times faster than real time for a simulation forced by tide only and including sediment transports. This ratio is heavily dependent on the computer that is used for the simulation. If possible, the simulation time should remain within 12 hours, since this would allow simulating many model cases, without much waiting time. For the new model with a single representative tidal cycle this means the model should calculate at a ratio of around 1:1.

For the refined model a new timestep has to be calculated. The timestep should be chosen as large as possible without influencing the stability of the model. The maximum timestep can be determined based on the Courant-Friedrichs-Lewy number (CFL):

$$CFL = \frac{\Delta t \sqrt{gH}}{\{\Delta x, \Delta y\}} \quad (4.1)$$

Where Δt is the timestep, g the gravitational acceleration, H the water depth and $\{\Delta x, \Delta y\}$ a characteristic value of the grid spacing in either direction (Deltares, 2013). A decrease of grid

cell length (x or y) should therefore result in a timestep reduction of a similar factor.

The first estimate of the timestep is based on the change in grid cell size in the area of interest. The grid cells were reduced from around 160 by 60m to 25 by 25m. This is a reduction of a factor 5, which results in a timestep of 1.5 seconds.

A further reduction is possible, since the NeVla model has a higher resolution further into the estuary compared to the outer delta. The optimal timestep has been investigated by comparing model results for different timesteps (see Figure 4.3). No significant change in model results is observed for a timestep of 6 seconds. This timestep is therefore used for further simulations. The ratio between simulated and real time is around 5.4.

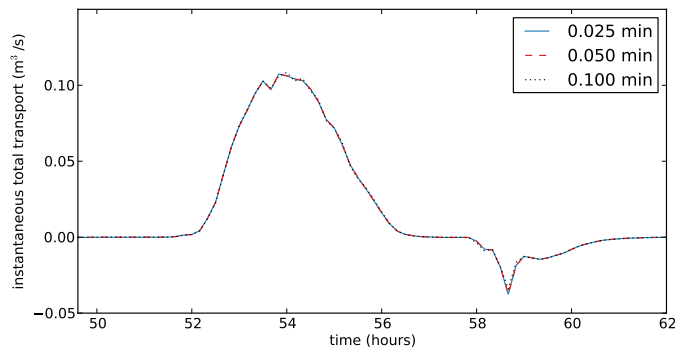


Figure 4.3: Comparison of instantaneous total transports through a cross section in the Oostgat tidal channel for different timesteps

4.4 Additional model settings

Important model settings that have been used similar to the existing Delft3D-NeVla model are shown in table 4.2. See the report by [Tonnon and Van der Werf \(2014\)](#) for more details.

Table 4.2: Model settings

Setting	Value
Bathymetry	2011
Roughness	type Manning value 0.024
Grain size	0.2 mm
Transport formulation	Van Rijn 2004

5 Model results

In this chapter the model results are described. Several model cases have been calculated. In the first section the results of these cases are described. The next section compares the different cases based on the erosion at the coastward channel slope. Based on these results, the most important forcing mechanism (tide, waves or wind) is concluded.

5.1 Model cases

For the estimate of the importance of wind, waves and tide different model cases are created. The first model case aims at approximating the actual sediment transports as much as possible by including tide, waves and wind as the main forcing mechanisms (C1). The most important mechanism for forcing the water level and flow velocities is the tide. The alternating directions cause large sediment transports in both directions with a limited net effect. The second case focuses on determining the net effect of this tidal movement (C2). Additional cases with tide and waves (C3) and with tide and wind (C4) are executed to determine the effect of waves and wind separately. Case C3 does not contain waves, which does not occur in reality. The simulated cases are included in Table 5.1. The simulations with wind also include wind induced setup.

Table 5.1: List of model cases and included forcing mechanisms

Case	Tide	Waves	Wind
C1	x	x	x
C2	x		
C3	x	x	
C4	x		x

5.1.1 Tide, waves and wind (C1)

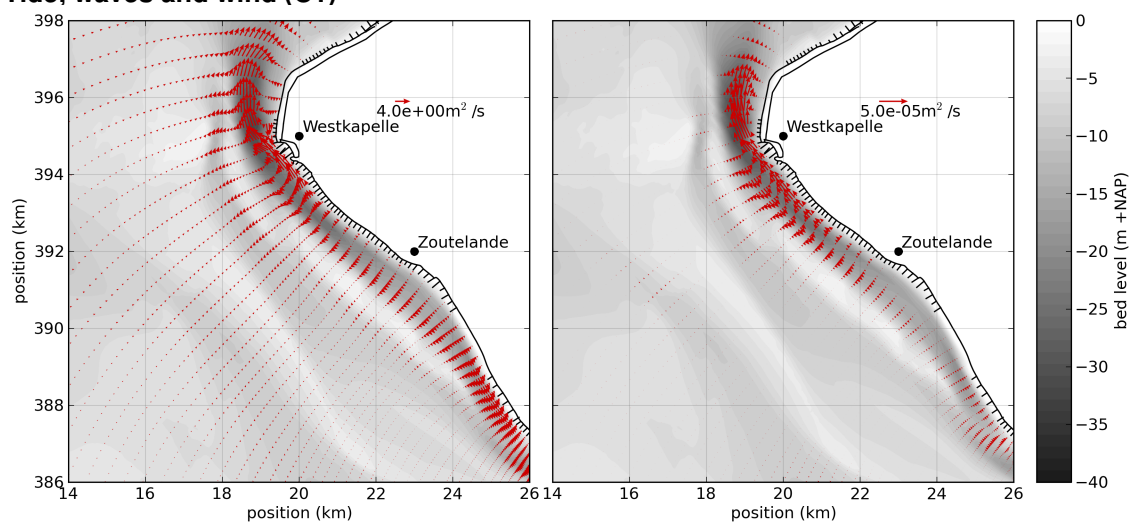


Figure 5.1: Net specific discharge (l) and residual transport (r) for model case C1 which includes tide, waves and wind

The model simulation which includes forcings by tide, waves and wind resulted in net discharges and transports as shown in Figure 5.1. There is a net discharge per tidal cycle across the banks towards the coast. This occurs mainly at the northern section of the 'Bankje van Zoutelande'. In the Oostgat the water is discharged both to the north and south which creates a residual ebb flow in the northern section and a flood flow in the southern section. The two flows diverge behind the 'Bankje van Zoutelande'. The ebb flow is more dominant at the coastward side while the flood discharge is more dominant along the banks.

The most important sediment transport pattern is the ebb-directed sediment transport at Westkapelle with a divergence along the coastward channel slope towards Westkapelle. This matches to the location where erosion was measured. Along the seaward channel slope sediment is transported to the south towards the Sardijneul. Finally, there is an ebb-directed sediment transport through Oost Deurloo. An important result is the difference between the discharge towards the coast and the sediment transports which have a minor coastward directed component. Most sediment transport is parallel to the channel. The residual transport directions are similar to the net discharge directions, whereas the transport magnitudes show more significant differences to the discharge magnitudes.

These results are mostly consistent with the transport patterns that were found by Erkens (2003). The transport directions in model results match well to the directions derived from the directions of the sand waves. Larger differences are found in the transport magnitudes. The sediment transport in the model along the 'Bankje van Zoutelande' is of the same order of magnitude as the ebb-directed transport on the coastward side of the channel, whereas Erkens shows a much larger transport. The uncertain flood-directed transport in Oost Deurloo from the study by Erkens is also visible in the model results. Sediment transports near the Sardijneul show larger differences. This area is close to the model boundary which might explain some differences.

5.1.2 Tide (C2)

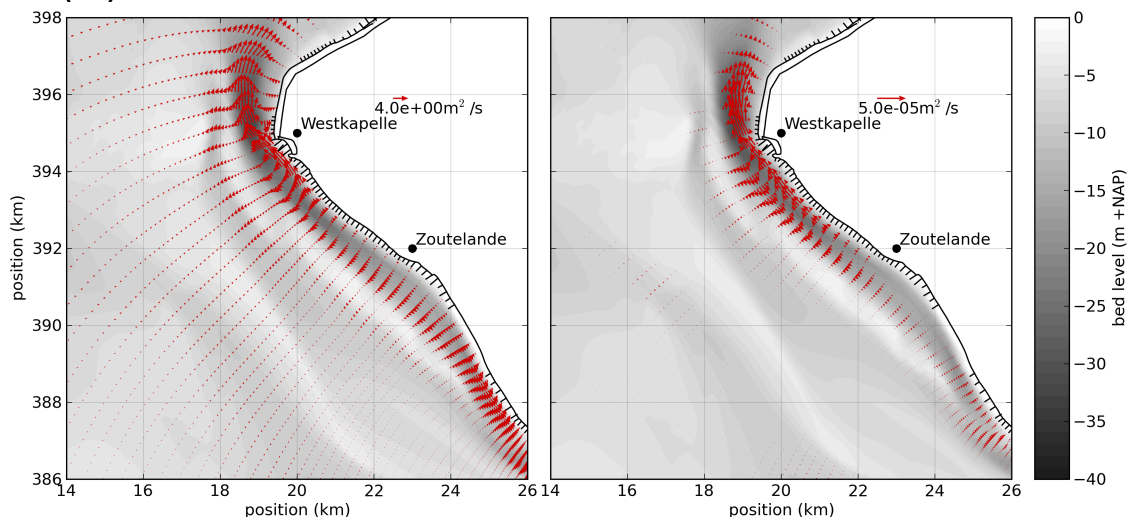


Figure 5.2: Net specific discharge and residual transports for model case C2.

In this section the model results for model case C2 with tide as the only forcing mechanism on the system are described. Figure 5.2 contains the specific discharge and transport for this model case. The different stages of the M2 tidal cycle and related transports are described. This provides insight into the importance to sediment transports for different phases in the tide. The phase of the tide is based on the water level at Westkapelle.

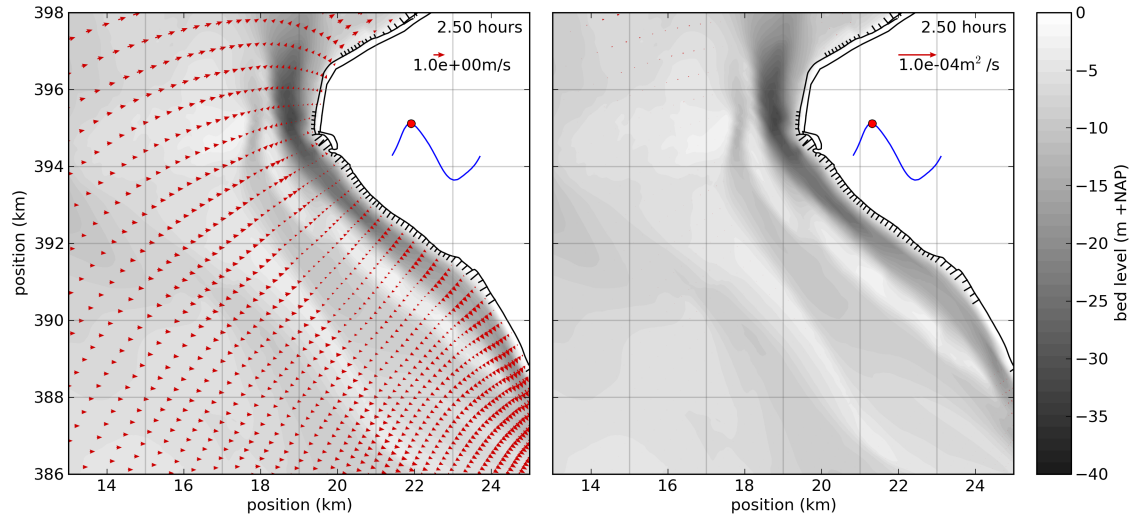


Figure 5.3: High tide with flow velocities (l) and instantaneous transports (r)

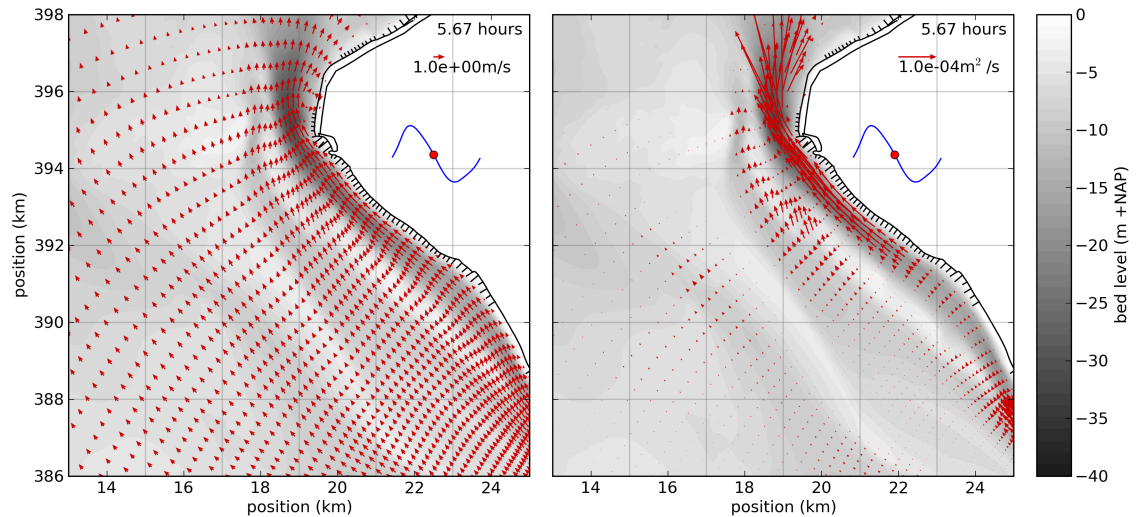


Figure 5.4: Ebb tide with flow velocities (l) and instantaneous transports (r)

When high tide (Figure 5.3) is reached at Westkapelle, the tide is still rising at the Sardijngeul, which causes a southward directed flow in the southern part of the channel. To the north of the Oostgat the tide is already lowering, which causes an ebb-directed flow towards the north. Finally, there is an onshore-directed flow from the 'Vlakte van Raan'. Transports are limited during this stage of the tide.

As the water level recedes during ebb tide (Figure 5.4) the flows are directed towards the north. Large flow velocities occur in the northern section of the channel. A return flow occurs at Westkapelle on the coastward side of the channel past the bend. Flow velocities across the banks also have an onshore component. A large sediment transport gradient can be observed in the channel with small transports in the southern section and very large transports in the northern part. There is also a northward directed sediment transport in Oost Deurloo.

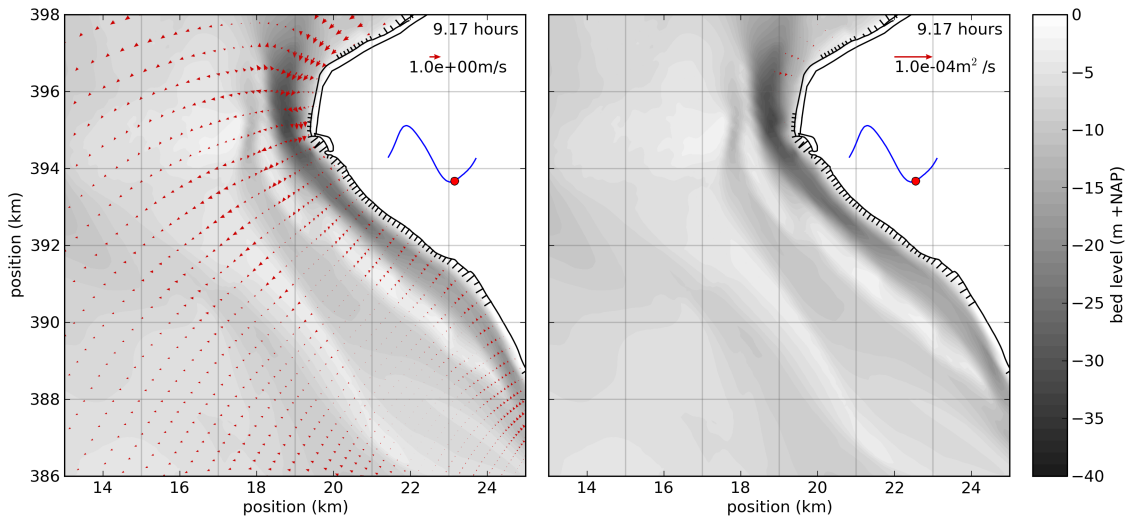


Figure 5.5: Low tide with flow velocities (l) and instantaneous transports (r)

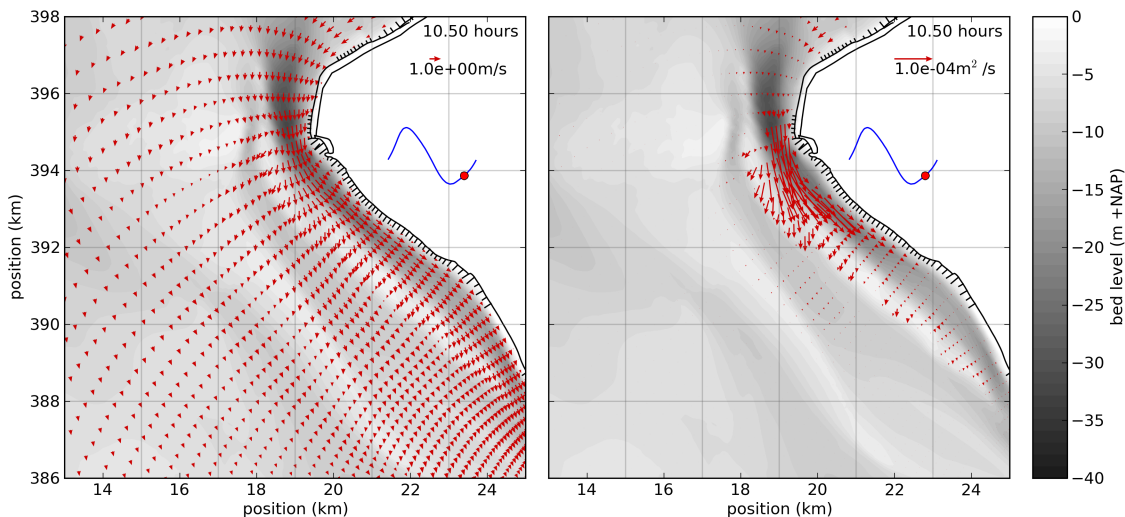


Figure 5.6: Early flood tide with flow velocities (l) and instantaneous transports (r)

During low tide (Figure 5.5) velocities in the study area are limited. A southward directed flow is located to the north of the channel and there is a small offshore directed flow across the banks ('Bankje van Zoutelande' and Elleboog).

During early flood tide (Figure 5.6) a significant transport occurs from the Oostgat across the banks in offshore direction with large sediment transports. Flow velocities through the tidal channel are relatively constant from north to south. At a later stage of the flood tide (Figure 5.7) the transport across the banks has decreased again and the sediment transport in the channel has increased.

The transports during ebb and flood are all in longshore direction. Cross shore flows and transports occur at periods of low flow velocities during high tide, low tide and the first phase of flood tide.

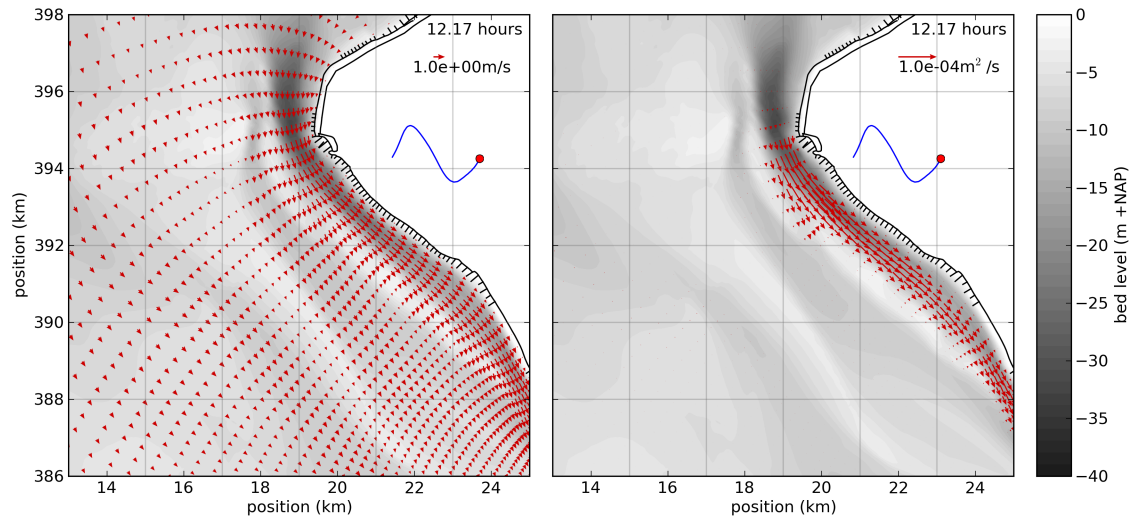


Figure 5.7: Flood tide with flow velocities (l) and instantaneous transports (r)

5.1.3 Tide and waves (C3)

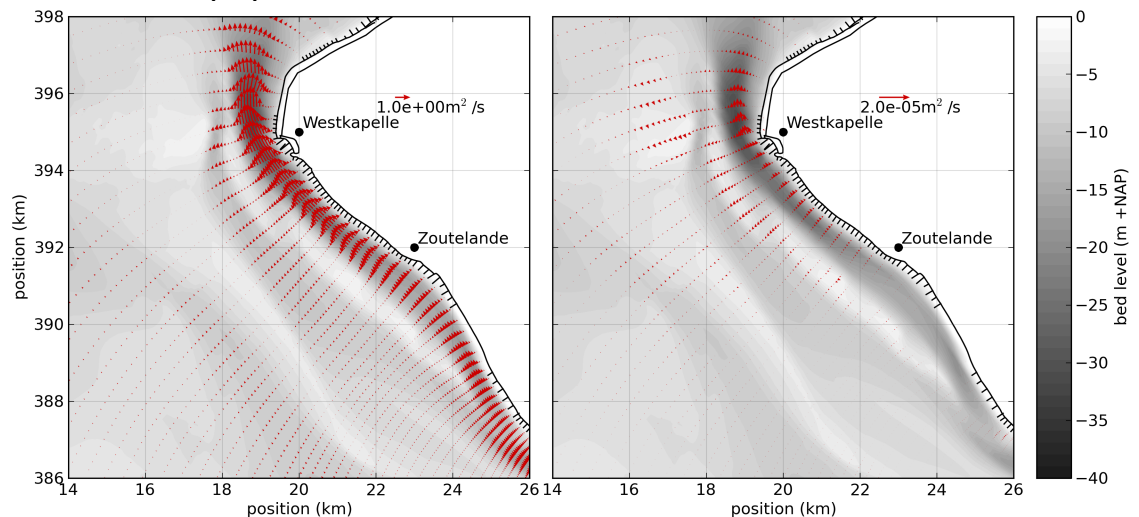


Figure 5.8: Net specific discharge and residual transports for model case C3 with the effect of tide (C2) subtracted from the results

The net discharge and residual velocity for the representative wave climate are shown in Figure 5.8. Since the wave climate of the Dutch coast mainly consists of waves from the southwest and northwest, wave conditions from these directions are also discussed using the net effect of discharge and transports over the tidal cycle. Finally, a western storm condition is included in the representative wave climate.

The combination of wave conditions in the representative wave climate results in an additional ebb-directed discharge both through the Oostgat and Oost Deurloo. The sediment transports show an ebb-directed transport along the coast with an increase in transports between Zoutelande and Westkapelle. These transports are small compared to the tide driven transports as shown previously. Some transport at the banks is visible. Discharges at these locations are not much higher compared to tide driven velocities. These transports are caused by dissipation of wave energy at the shallow parts of the system. These transports are in coastward direction and occur mainly at the Rassen and the northern section of the 'Bankje van Zoutelande'.

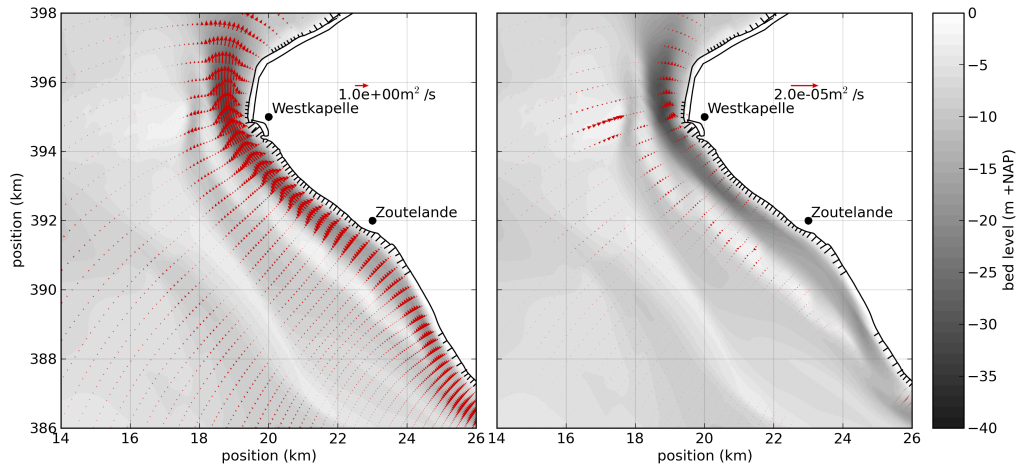


Figure 5.9: Net specific discharge and residual transports for southwestern wavecondition ($H_s=1.88m$, $Dir=231^\circ$, $Weight=16\%$)

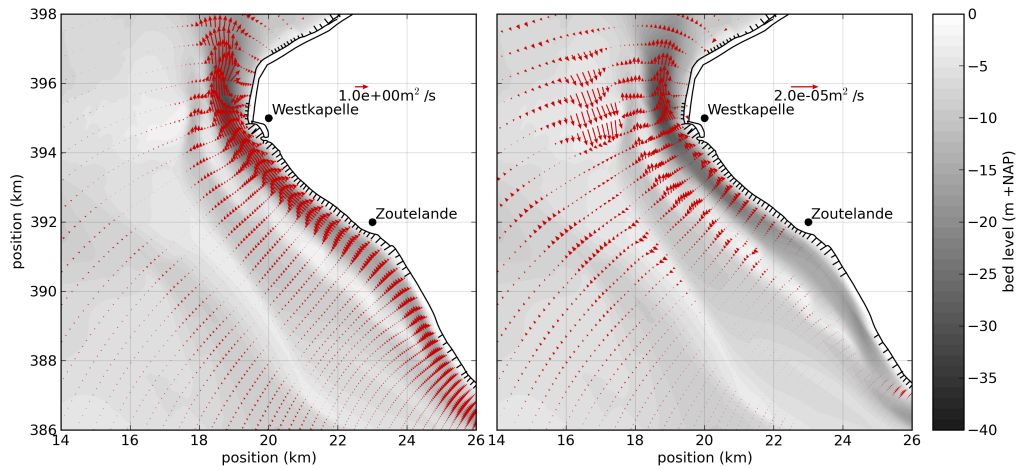


Figure 5.10: Net specific discharge and residual transports for northern wavecondition ($H_s=1.31$, $Dir=357^\circ$, $Weight=3\%$)

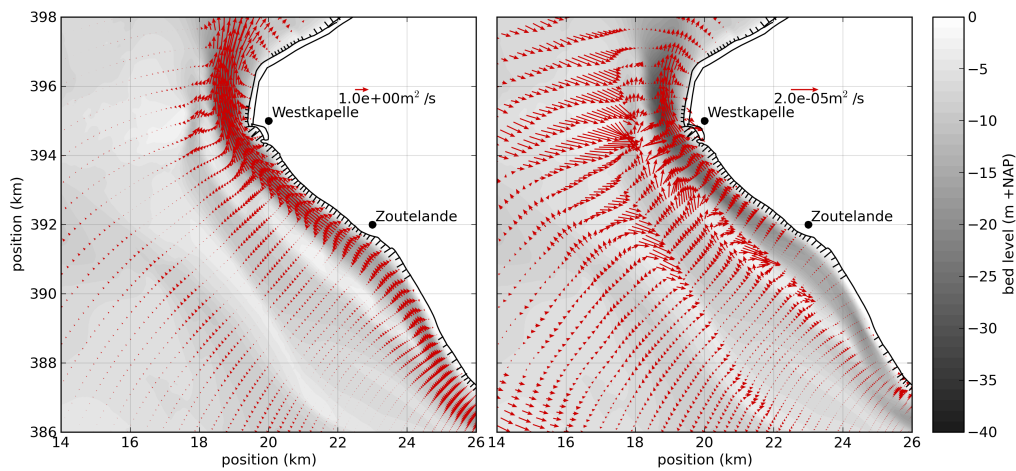


Figure 5.11: Net specific discharge and residual transports for storm wavecondition ($H_s=2.38$, $Dir=285^\circ$, $Weight=5\%$)

The southwestern wave condition has very little influence on the sediment transports. The northward directed transport at Westkapelle is stronger than for tide only. The transport at the Rassen is the most remarkable effect for this wave condition. Where tide did not influence the transports at the Rassen, the southwestern waves cause a coastward directed transport at the Rassen.

The northern waves have more effect on the sediment transports. They still cause a northward transport in the Oostgat and at the northern part of the 'Bankje van Zoutelande'. There is a southward directed transport in a similar direction to the waves at the Rassen and Elleboog.

A wave condition with high waves from the west causes a strong northward discharge in the channel. The transports show a dominant wave driven transport at the Rassen, Elleboog and 'Bankje van Zoutelande' in southeastern direction. The northern section of the 'Bankje van Zoutelande' has a northward directed transport which is strongest between the two sections of the bank. This results in a strong divergence of transports at the northern point of the southern section of the 'Bankje van Zoutelande'.

5.1.4 Tide and wind (C4)

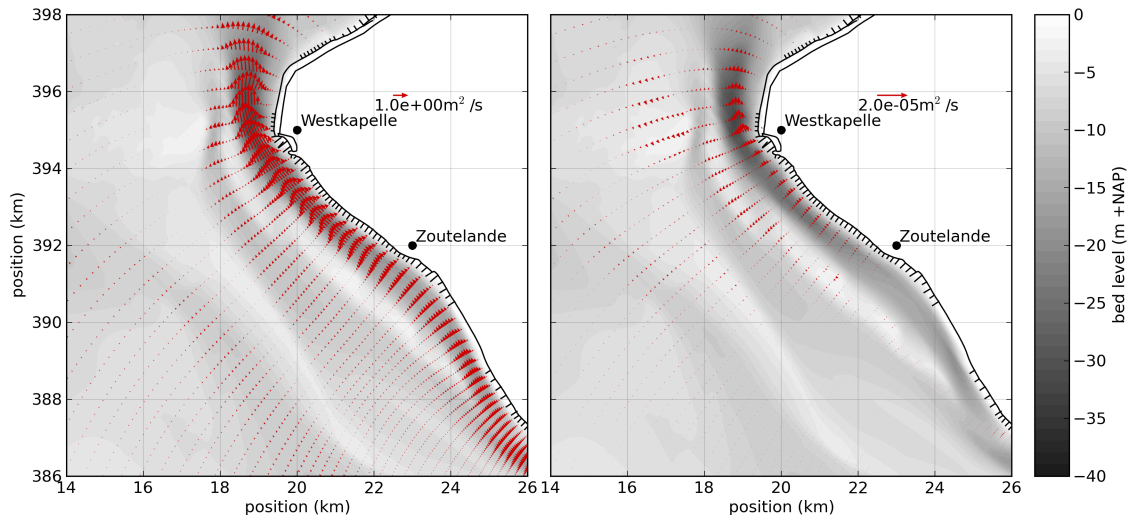


Figure 5.12: Net specific discharge and residual transports for model case C4.

The wind climate results in an additional discharge towards the north in the channel. The effect of wind on sediment transports is found in the channel (small additional northward transport) and on the Rassen and 'Bankje van Zoutelande'. The transport on the Rassen is directed in longshore direction towards the southwest and the transports at the 'Bankje van Zoutelande' are towards the north.

Both the stormy western and southwestern wind conditions cause strong transports in the ebb tidal system towards the northeast with transports focused in the Oostgat and 'Bankje van Zoutelande'. The northern wind condition results in a southward directed discharge and transport. These are smaller in magnitude which might be due to the lower wind velocities for this condition.

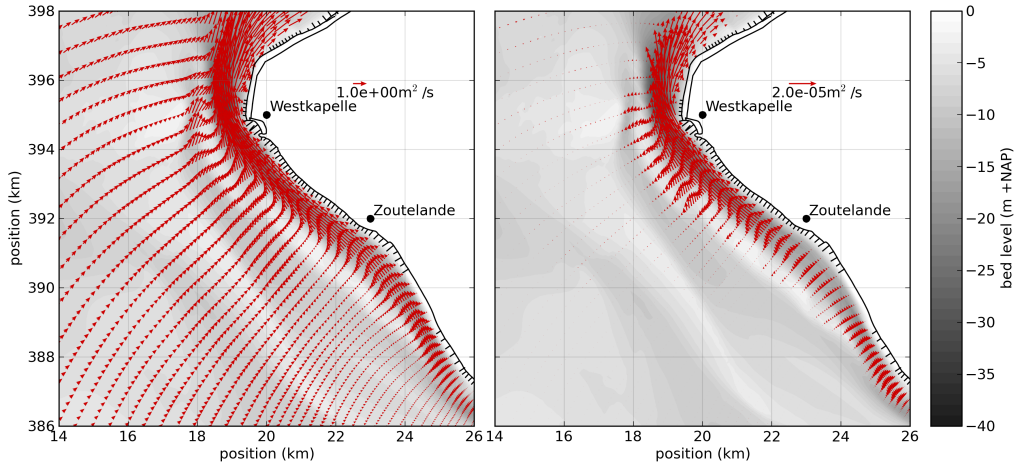


Figure 5.13: Net specific discharge and residual transports for southwestern windcondition (Surge height=0.10m, Speed=10.71m/s, Dir=231°, Weight=16%)

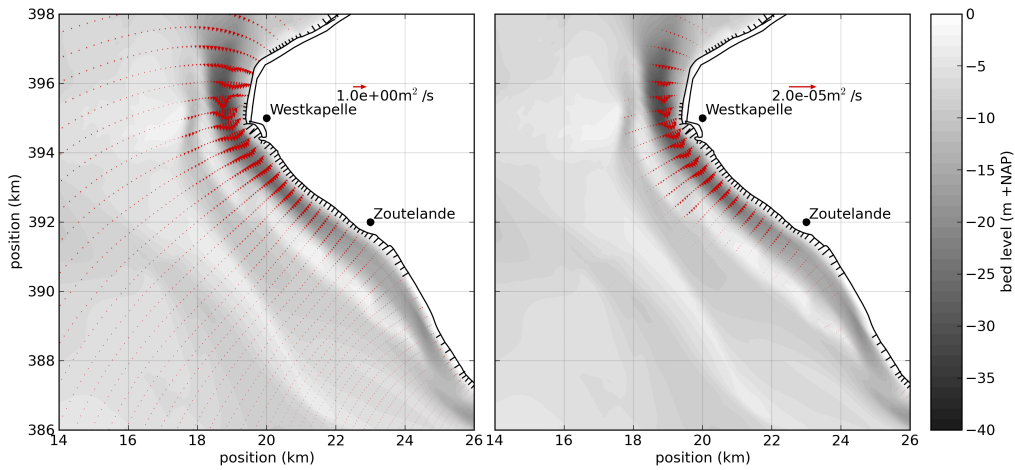


Figure 5.14: Net specific discharge and residual transports for northern windcondition (Surge height=0.07m, Speed=6.64m/s, Dir=350°, Weight=3%)

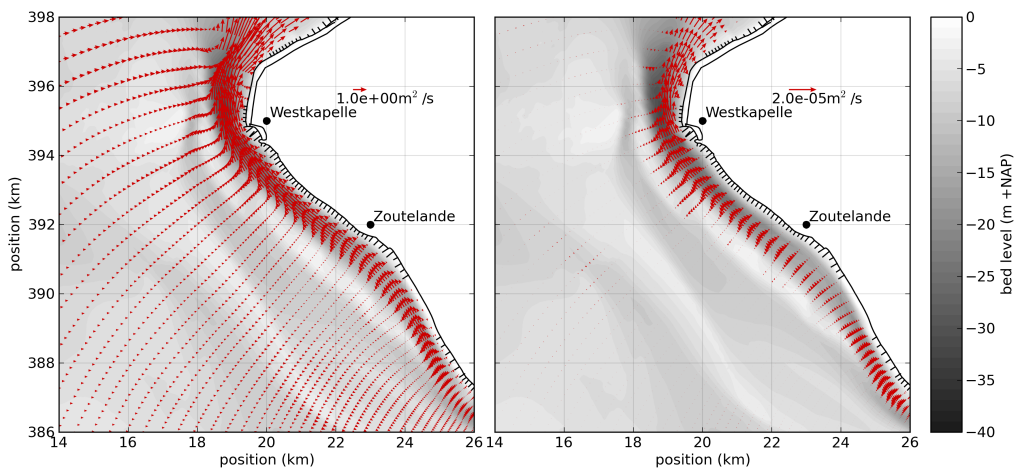


Figure 5.15: Net specific discharge and residual transports for storm windcondition (Surge height=0.42m, Speed=10.78m/s, Dir=289°, Weight=5%)

5.2 Effect of tide, waves and wind on erosion at the channel slope

The erosion at the coastward channel slope is evaluated using the change in sediment volume within control volumes (see Figure 5.16).

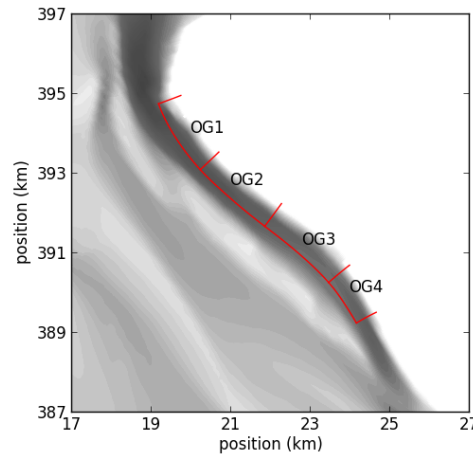


Figure 5.16: Control volumes OG1-OG4 at the coastward channel slope of the Oostgat that are used for evaluation of the net sediment volume change over a tidal cycle.

Figure 5.17 shows the change in sediment volume within the control volumes. The effect of the tide has been derived directly from the second case. Wind and wave driven transports were obtained by subtracting the effect of the tide from the third (tide and wind) and fourth case (tide and waves).

When multiple forcing mechanisms are included in a single simulation there are likely to be interaction effects between these mechanisms. Since the tide is always present as a forcing mechanism, the interactions with wind and waves cannot easily be excluded when calculating the effect of a single component. The interactions of the tide with other forcing mechanisms is therefore not extracted from the components. The interaction of wind with waves is calculated as the difference between the erosion in the first case (C1), which includes all forcings and interactions, and the effect of the separate components tide, waves and wind.

The case which includes all implemented forcing mechanisms (tide, waves and wind) shows erosion in all four control volumes. The strongest erosion effect occurs in OG2 and OG3. Tide (C2) is the main contributor to the coastal erosion at the channel slope, while waves (C3) and wind (C4) have a much smaller effect. Both wind and waves are expected to have a larger effect in shallow water. Wind is forced at the surface and waves can cause transports when they start to shoal and break in the surf zone. This might explain the relative importance of the tide at the channel slope since the slope extends to large depths. The transport pattern due to waves can be explained by the shape of the coast. The waves at the Dutch coast arrive from the northwest or southwest which, due to the orientation of this section of the coast is parallel or normal to the coast, whereas an oblique angle is required for wave driven transport.

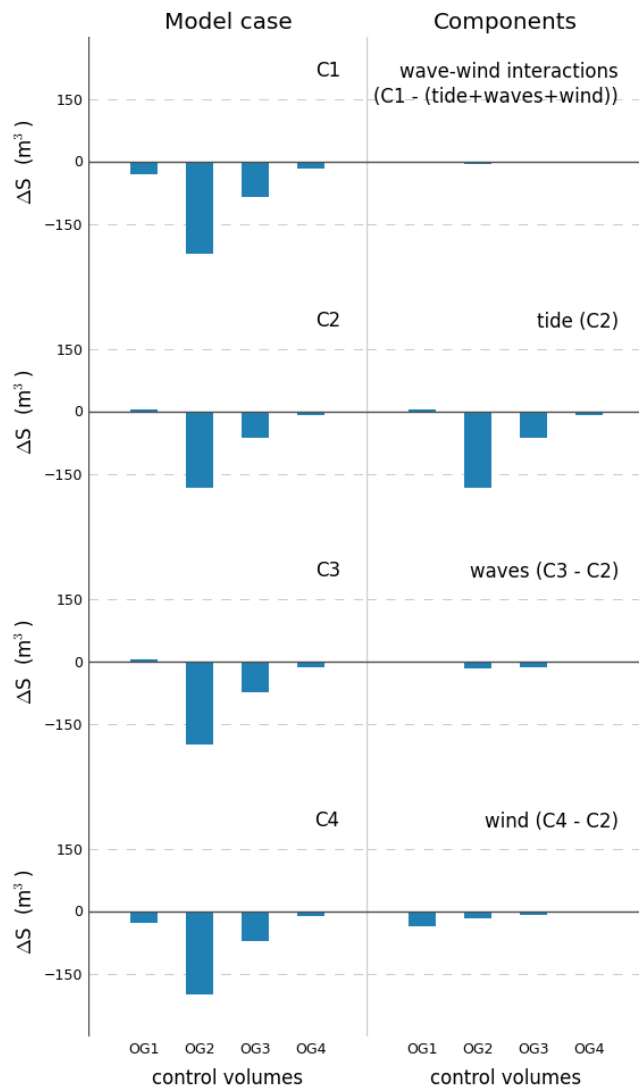


Figure 5.17: Change in sediment volume within different control volumes for multiple model cases and the derived net effect caused by tide, wind and waves. Individual components for wind and waves are derived by subtracting the effect of tide from the model case data.

6 Conceptual model

The model results contain a coastward transport divergence between Zoutelande and Westkapelle which results in erosion as follows from equation 6.1.

$$\nabla \cdot \vec{q} + \alpha \frac{\partial z}{\partial t} = 0 \quad (6.1)$$

with \vec{q} the sediment transport rate, t time, z the bed level and α an arbitrary constant. In this chapter a conceptual model is formulated that is able to explain this erosion pattern at the channel slope. There are differences in transport patterns due to waves and wind when compared to tide driven transports, but these differences are small. Therefore, the conceptual model is limited to explaining the tide driven transport patterns that affect the erosion at the channel slope.

Changes in channel discharge as well as the transport magnitude and direction at the 'Bankje van Zoutelande' are analyzed since these processes are related to the erosion mechanisms as discussed in Chapter 3.

6.1 Channel discharge comparison 1973-2011

Changes in discharge over the last decades can lead to increased erosion, which has been explained in Section 3.3. When the discharge increases, flow velocities increase, which results in erosion at the cross section. Eventually a new balance can be reached when the cross sectional area has increased enough to decrease velocities to the point that erosion no longer occurs.

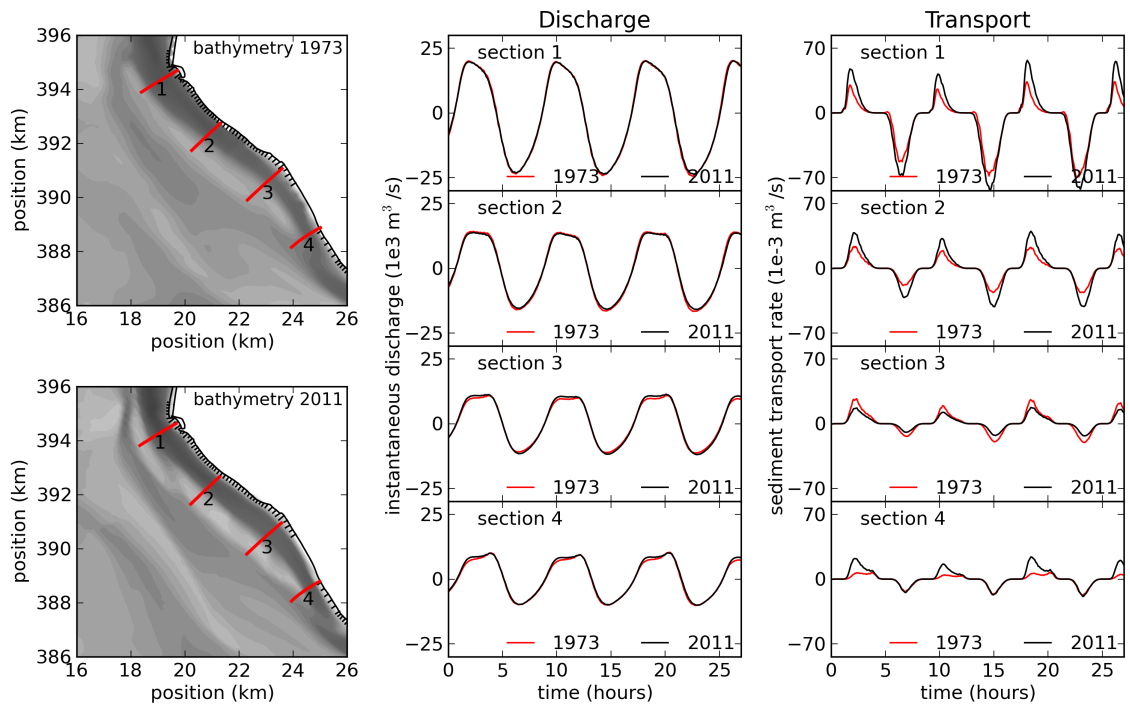


Figure 6.1: Comparison of discharge and transport through tidal channel Oostgat between 1973 and 2011

The bathymetry for the simulation of 2011 has been changed to data from 1973 (boundary conditions have been derived from the larger Delft3D-NeVla model with the bathymetrical data of 1973). The results in Figure 6.1 show no large differences between the discharges of model results for 1973 and 2011. Discharges at cross sections 3 and 4 have increased, while discharge at cross section 2 has decreased. The changes in sediment transport rates at these locations show different trends, with transports at section 3 having increased while discharges have decreased. It is therefore more likely that other processes have led to the changes in transports.

Bathymetrical changes might explain the differences. Even though the discharge has not changed significantly, the channel width and depth and thus the cross sectional area of the channel have changed. This will influence the velocity patterns and sediment transport rates.

6.2 Sediment flux across 'Bankje van Zoutelande'

Model results show a net discharge across the 'Bankje van Zoutelande'. As explained in section 3.1 the sediment transport across the bank can cause coastal erosion. This transport is studied to estimate the importance of this mechanism to the coastal erosion of the Oostgat.

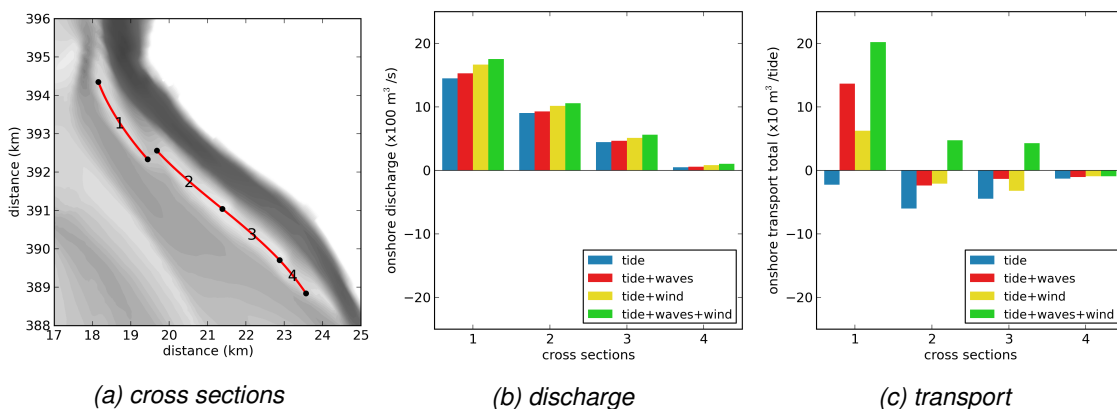


Figure 6.2: Evaluation of bank transport over a tidal cycle

The net discharge across the 'Bankje van Zoutelande' for each model case is displayed in Figure 6.2b. It shows a significant discharge across the banks, but this does not cause a tide driven onshore transport as might be expected (Figure 6.2c). The different directions of tide driven discharge onshore and sediment transport offshore can be the result of several factors:

- ◇ The water depth during high tide is larger which means that a larger discharge at high tide does not imply larger flow velocities compared to low tide. Not discharge but flow velocities (at the bed) are most important to the sediment transport rates (time lag between water level and flow velocities).
- ◇ Peak velocities during ebb tide can cause a net transport in opposite direction from the transport caused by residual discharge and velocity (tidal asymmetry).
- ◇ The sediment that is stirred during peak flows can be transported away after the velocity has changed direction. This process might therefore cause a transport in opposite direction to the instantaneous velocities (time lag between pickup and deposition of sediment).

A different pattern occurs when including waves or wind in the simulation. The offshore transport for cross sections 2-4 is reduced and when both forcing mechanisms are included, the transport

direction reverses. The onshore direction of wind and wave driven transport processes can be expected, since both have a dominant southwest to northeast direction. In addition, waves can break at the banks during storm conditions, causing strong onshore-directed sediment transports. Wind adds a shear stress on the water surface. The effect of this shear stress is limited at locations where the waterdepth is large, but at shallow locations such as the banks in front of the coast, this can have significant impact.

The tidal flow is not responsible for an onshore-directed sediment flux across the 'Bankje van Zoutelande'. The addition of waves and wind driven transports results in a small onshore transport. It is not likely that the small sediment transport at the bank is responsible for the strong coastward sediment divergence that causes the erosion. The narrowing of the channel due to sedimentation at the bank should increase flow velocities across the entire channel, while the divergence of transports occurs on the coastward side of the channel. A possible cause of the limited influence of this mechanism to the coastal erosion is related to the large flow velocities in the channel compared to the rest of the system. As sediment is transported across the banks, the tidal flow flushes the sediment away and therefore prevents the sedimentation at the bank and thus the narrowing of the channel.

6.3 Decomposition of velocities

The tide alternates directions every tidal cycle. The residual flow velocity over this period is therefore much smaller than the actual velocities during the cycle which means transport due to the residual flow is therefore not necessarily dominant in tide dominated areas. Transport of sediment over a tidal cycle can be approximated by equation 6.2.

$$\mathbf{q} = \alpha \mathbf{v} |\mathbf{v}|^2 \quad (6.2)$$

with \mathbf{q} the sediment transport, α an arbitrary constant and \mathbf{v} the flow velocity vector. By decomposing the velocity in a time averaged component ($\bar{\mathbf{v}}$) and velocity fluctuations ($\tilde{\mathbf{v}}$) with an average of zero (see equation 6.3) equation 6.4 can be derived (see appendix E) where the time averaged value is shown with $\langle \rangle$. This decomposition of velocity driven transport has been performed for a one-dimensional case by Rocha *et al.* (2013) and Roelvink and Stive (1989).

$$\mathbf{v}(t) = \bar{\mathbf{v}} + \tilde{\mathbf{v}}(t) \quad (6.3)$$

$$\frac{\langle \mathbf{q} \rangle}{\alpha} = \bar{\mathbf{v}} |\bar{\mathbf{v}}|^2 + \bar{\mathbf{v}} \langle |\tilde{\mathbf{v}}|^2 \rangle + \langle \tilde{\mathbf{v}} |\tilde{\mathbf{v}}|^2 \rangle + \langle 2\tilde{\mathbf{v}} (\bar{\mathbf{v}} \cdot \tilde{\mathbf{v}}) \rangle \quad (6.4)$$

Since suspended transport is strongly related to the bed load and the combination results in the total transport, this approximation can offer an indication of the real transports. By making a comparison with both the bed load and total transport as they resulted from the model, the quality of the approximation can be estimated. This approximation does not include effects such as bed slope effects and the velocity required for initiation of motion of sediment.

The approximation of transports (Figure 6.3b) is very similar to the bed load transports (Figure 6.3a) and shows a good representation of transport directions compared to the total tide driven transports in Figure 5.2. Locations with higher and lower transports also relate well to the residual transports. There are some differences in scale which can mostly be attributed to

the suspended sediment transport. Since the patterns are more important for this study than the actual magnitude of the transports, it is concluded that the decomposition of the approximation into multiple velocity driven processes of sediment transport give good representations for the real sediment transport components.

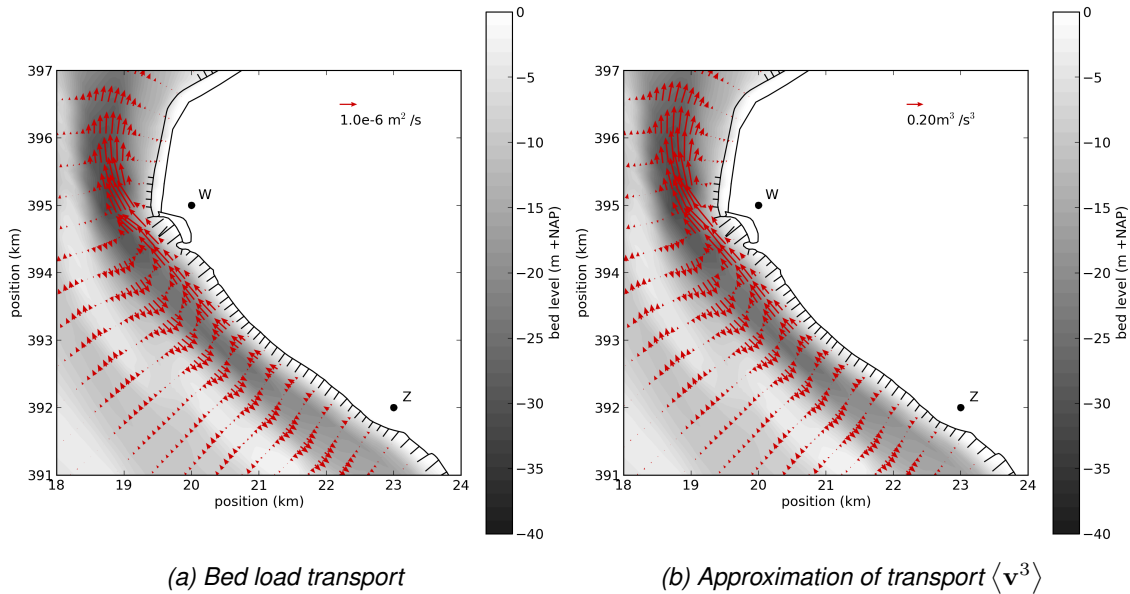


Figure 6.3: Comparison an approximation based on tide driven velocities to the bedload transport due to tide

The equation contains four components that together describe the transport approximation. By analyzing these components, the cause of the coastward erosion can be narrowed down to one or more physical processes that are related to the mathematical representation of the components. The first component in Eq. 6.4 represents the transport as a result of the residual velocity. Due to the alternating directions in the tidal flow velocities, the residual velocities are small and this component has a minor contribution to the total transport (Figure 6.4a). The second component (Figure 6.4b) represents stirring of sediment by velocity fluctuations and transport by the residual velocity. This component shows a significant contribution to the transports and a minor longshore gradient. The third component (Figure 6.4c) contains the transport due to velocity skewness. The peak velocities during ebb near the coast cause higher transports. The final component (Figure 6.4d) represents a correction on the velocity skewness if the skewness is along the path of the residual transports. Since the total velocity is a combination residual velocities and velocity fluctuations, the third power of the velocity is higher when the velocity fluctuation is in the direction of the residual flow. This is therefore an important interaction for the calculation of the sediment transports.

These results show that the correction on the velocity skewness is the main contributor to the velocity driven erosion at the channel slope of the Oostgat. The results also show an opposite flood-directed transport at the seaward side of the channel which implies an imbalance in the tidal flow velocity between both sides of the channel which drives the sediment transport.

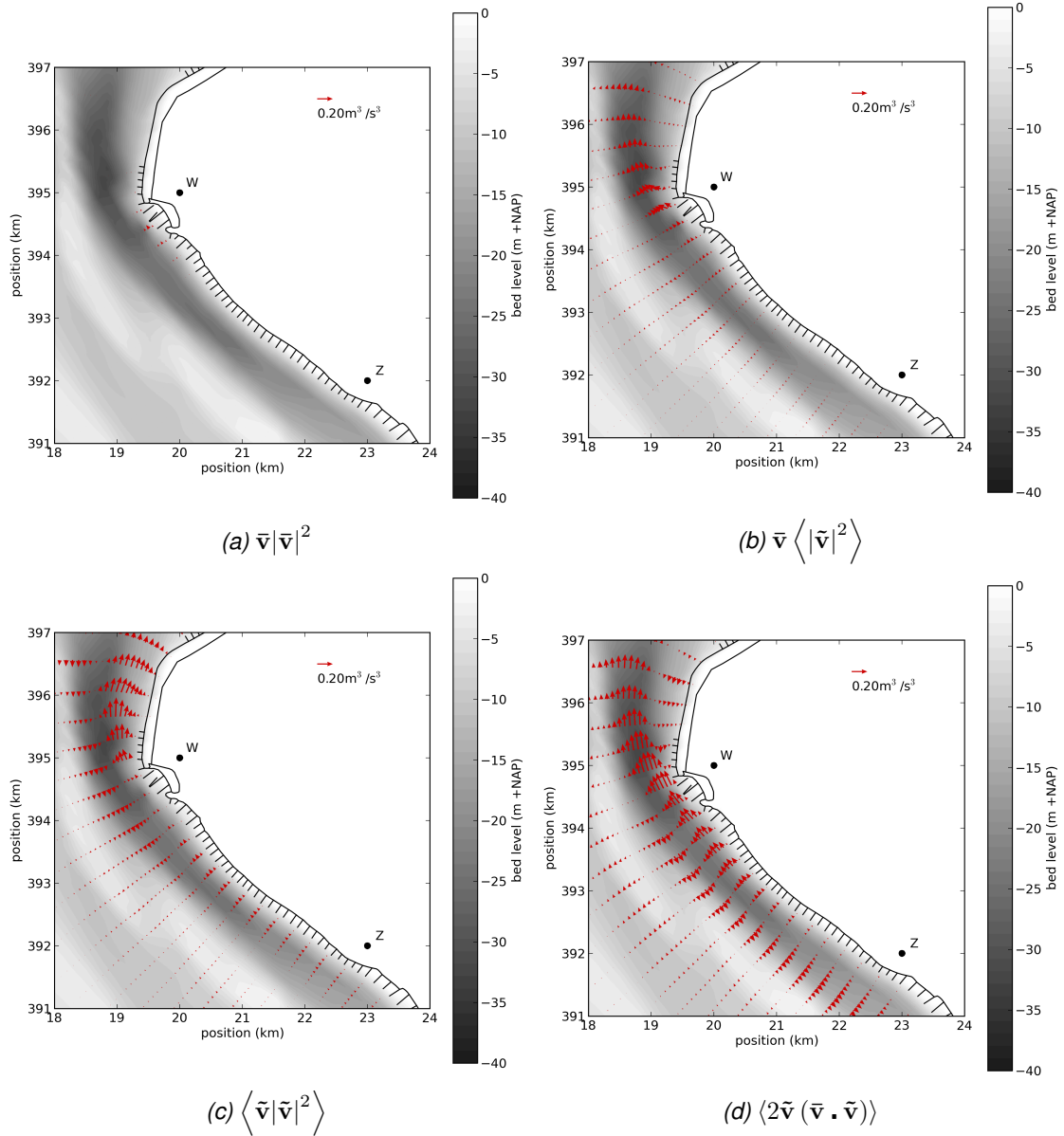


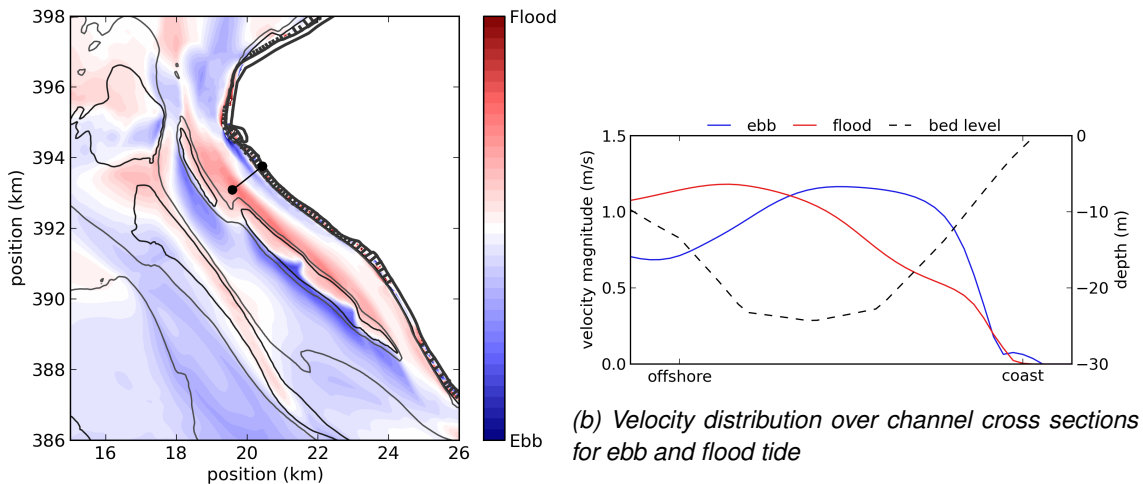
Figure 6.4: Components of velocity driven transport approximation $\langle v^3 \rangle$

6.4 Dominance of tidal flows

The tidal dominance (defined as the ratio between maximum ebb and flood velocities at each location) is shown in Figure 6.5a. Oost Deurloo is ebb dominated with the strongest dominance directly behind the ‘Bankje van Zoutelande’. These patterns suggest that the bank is shielding those areas from the flood tide and consequently the ebb tide becomes more dominant.

The channel Oostgat contains several parts that are clearly either ebb or flood dominant. The southern part near the Sardijnegeul is flood dominant, which matches with the net discharge in flood direction in this section. The coastward side of the channel at Westkapelle is ebb dominant and the seaward side of the channel at Westkapelle is flood dominant. These observations are consistent with the concluded imbalance in tidal flow velocities across the channel from the previous section. The flood dominance at the seaward side can be explained by the inertia of the flow around the bend. Due to high flow velocities during flood tide the flow cannot maintain a rotation around the bend and is ‘pushed’ to the seaward side of the channel. In addition, the

flood tidal flow has a component in longshore direction towards the sardijnegeul and a cross shore direction across the banks (overflow due to decrease in depth and discharge of the channel towards the south). The velocity magnitude is therefore larger at the seaward side of the channel resulting in more sediment transport. Due to the concentration of the flood tide at the banks the ebb tide becomes more dominant in the inner bend, causing a net transport with the ebb flow at the coast.



(a) Tidal dominance based on a comparison of maximum ebb and flood velocities

Figure 6.5: Imbalance of tidal flows with tidal dominance (ratio between maximum ebb and flood) and cross shore velocity distribution. For the tidal dominance the ebb and flood have been differentiated based on the flow direction with ebb direction the longshore component towards the north and flood the longshore component towards the south.

The velocity distribution for a cross section just south of Westkapelle is shown in Figure 6.5b. These results confirm the concentration of the flood tide at the seaward side. This figure also shows the shift of the ebb tidal flow towards the coast, which has not been explained. The shift of the ebb flow further increases the ebb dominance and resulting erosion along the coastward side of the channel. Some effects that could cause the ebb tidal shift are:

- ◇ Contraction of the flow at the bend near Westkapelle that increases flow velocities at the coastward side
- ◇ Water level difference between the channel Oostgat and further along the coast to the north. Due to the divergence of the flow outside of the Oostgat the coastward flow velocities are accelerated along the coast to 'fill' the difference in water level.

These processes are not analyzed in this study but could be investigated using an idealized model that contains only the relevant processes.

6.5 Conclusion

In a study by [Erkens \(2003\)](#) the sediment transport patterns were described from an analysis of sand wave shapes on the bed of the channel (Figure 6.6a). Based on the model results for this study a new description of transport patterns is provided in Figure 6.6b. The main differences between the description by [Erkens \(2003\)](#) and the description from this study is around the 'Bankje van Zoutelande'. The transport magnitude along the coastward side of the bank is smaller. This also applies to the other sediment transports in the southern part of the Oostgat. The northward transport in Oost Deurloo is indeed found in the model results. The northward transport in the 'Geul van de Rassen' was not included in the previous description. Finally there is a small transport between both sections of the 'Bankje van Zoutelande'. The direction of this transport is highly dependent on the representation and accuracy of forcing mechanisms in the model.

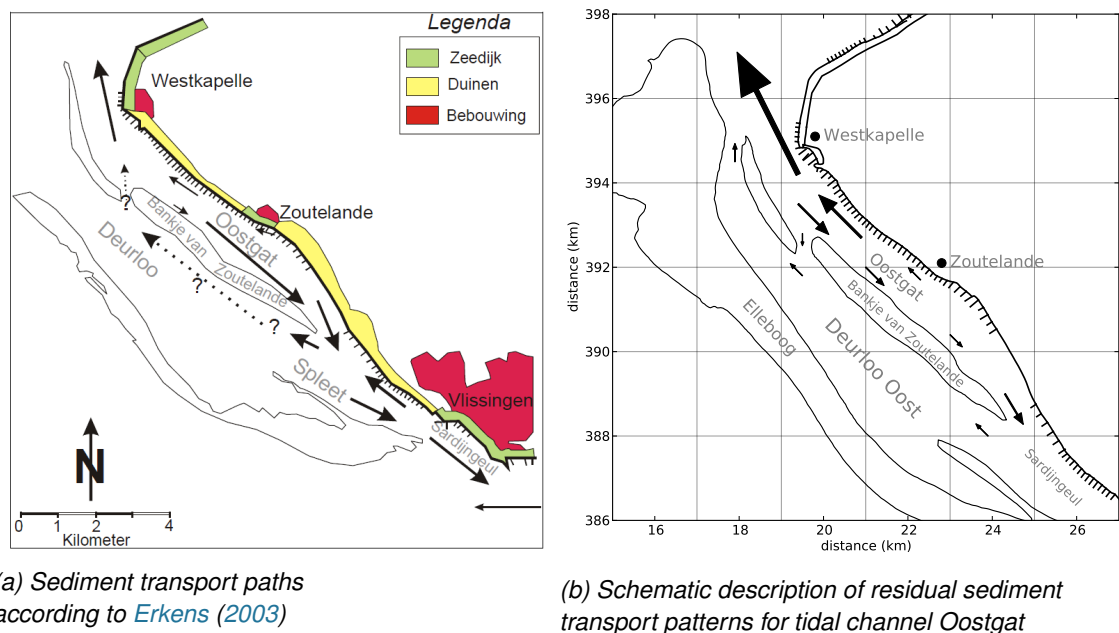


Figure 6.6: Comparison of transport pattern descriptions

In chapter 3 three erosion mechanisms were described. A lateral transport of sediment across the banks can lead to a migration of the bank. The sediment transport across the bank towards the coast has been found in model results, but only occurs when the model is forced by a combination of tide, waves and wind. The reduction in cross sectional area of the channel, due to the coastward transport of sediment leads to increased erosion along the bed. This effect should occur along the entire cross section, while modelled erosion occurs at the coastward slope. This effect could contribute to erosion of the channel, but is not the dominant erosion mechanism.

A divergence of flows behind the banks has been found in model results. There is a clear coastward directed net discharge. The northern section is ebb dominant while the southern section is flood dominant. This effect is likely to have an important contribution to the transports in the channel and the ebb-directed transports that are responsible for the coastal erosion, but the coastal erosion is also driven by a cross-channel imbalance of the flows which is not accounted for in this mechanism.

The final mechanism assumed an increase in channel discharge over time. An analysis of channel discharges between 1973 and 2011 showed no relation between changes in discharge and transports.

A net onshore discharge by the tide across the banks results in a divergence of flows and transports in the tidal channel Oostgat behind the 'Bankje van Zoutelande'. The northern section is ebb dominated whereas the southern section is flood dominated. Furthermore, there is an ebb dominance through the parallel channel Oost Deurloo/Geul van de Rassen.

In addition to these processes there is an unbalance of the tidal flow across the channel which is driven by several effects. The inertia of the incoming flood tide from the north around the bend at Westkapelle forces the flow towards the seaward side of the channel and across the 'Bankje van Zoutelande' which counters the transport due to the net onshore discharge. This effect causes a flood dominance at the seaward side of the channel.

The results show a strong coastward shift of the ebb tidal flow, with a coastward ebb dominance, which is not likely to be explained by the Coriolis effect alone. Possible processes that are responsible for the additional shift are contraction of the flow at Westkapelle and the water level gradient from Westkapelle to the north in combination with a divergence of the flow on the coastward side around the bend. These effects have to be investigated further.

7 Discussion

During this study many choices and assumptions were made that have an impact on the quality of the final results. These choices and the possible implications are discussed in this chapter as well as considerations to reduce the impact.

Delft3D can accurately model many aspects of the hydrodynamics in the Oostgat. Deviations from measurements can be reduced by a calibration procedure but it is usually not possible to produce a perfect match with the real situation. Due to sensitive relations between model properties these minor differences can result in significant deviations for other properties. Flow velocities are highly sensitive to changes in water level and sediment transports are in turn highly sensitive to flow velocities (third to fifth power). Furthermore, the bed level changes in Delft3D are sensitive to deviations in sediment transport. Finally, not all processes are included in Delft3D or are not feasible to implement in a model due to long calculation times. In this study the model and analyses have not included bed level change due to the uncertainty involved. By looking at patterns in flow velocities and sediment transports the instantaneous erosion can be evaluated.

The calibration of the Delft3D-NeVla model was based on water levels, discharges and current velocities. This means the sediment transports have not been calibrated and could potentially contain significant deviations from the real situation.

The model uses data from multiple sources. Each source has some uncertainty. Due to the sensitivity of the model results to changes in various parameters, as mentioned previously, this can have significant effects on the results. The bathymetry data from the original and more coarse NeVla model has been interpolated to the finer grid. Small bathymetrical elements are therefore not included in the model, which results in differences between model and reality. Since the patterns that are investigated are of a larger scale, the effect of this choice is expected to be limited.

Since the calculation time of the model should be limited to execute many different simulations, multiple assumptions have been made to reduce this calculation time. A representative tide has been identified to allow for the modelling of just one tide to reach a representative sediment transport. The main tidal variations occur within a cycle of 12.4 hours (M2) but there are many other tidal components with longer time scales that each can have a unique transport pattern. The M2 and S2 tides have the most significant contribution to the tidal amplitudes and the interaction forms the spring neap cycle. The original model included multiple spring neap cycles, but this was not considered feasible for the new model. Therefore the tide was reduced to a single representative cycle. By analyzing the correlation between sediment transports for each tidal M2 cycle and the average over the spring neap cycle the best representative tide was chosen. It is not possible to find a perfect tidal representation so there are differences between the net transport for a representative tide and actual yearly transports. These differences are not expected to have large impact, since they will likely not change flow patterns. The main difference between different tidal cycles will be in flow and transport magnitudes, for which the net effect is incorporated into the representative tide.

The wave climate is based on a binning procedure that was performed by [Van Rijn \(2012\)](#). In this study the choice was made to bin the data based on wind occurrences. While this choice resulted in an accurate representation of the wind climate, this results in a wave climate which does not accurately represent the actual wave climate. Southwestern waves are over-represented while

northwestern waves have a reduced occurrence. Furthermore, high waves are under-represented compared to low and medium waves. Since high waves are responsible for a relatively large portion of the sediment transport, the transports due to waves are expected to be larger in reality than is currently represented in the model. Since the erosion occurs at the channel slope, the effect of waves is not expected to have a large impact on the problem. Another issue that is related to the wave climate is the conversion of the binned wave climate to the representative climate. An approximation of the transports due to the waves in the entire climate is reached, but there are still expected to be differences in the transports (as is represented in the RMS in figure C.1).

3D effects have not been included into the model to save calculation time. These flows could have an important impact on the coastal erosion and transport patterns. To definitively eliminate 3D-effects from the processes that are important to the coastal erosion, a further study of this subject is required.

The approach of this study is based on reducing the important factors that influence the erosion at the Oostgat. Minor effects have therefore been left out of the analysis at every stage. Possible cumulative effects of minor processes that together have a significant effect are therefore not caught.

The model grid has been nested into the larger Delft3D-NeVla model. The quality of the new model has been estimated based on deviations compared to the calibrated Delft3D-NeVla model. Deviations from the NeVla model are either improvements due to a refining of the grid or cumulative errors due to the nesting procedure. A further analysis of measured data is required to better estimate the quality of the model.

The nested model had some issues with regards to the stability at the model boundaries. This required a complete revision of the model grid. The new grid performed significantly better than the first, but still contained some instabilities near the boundaries. The main instability was located in the Sardijneul and has probably influenced local flow patterns. Since the Sardijneul was outside of the area of interest, this has not been investigated further. The wave climate simulations had some stability issues as well. This was eventually solved by changing the direction of the waves by a single degree when necessary. Due to the uncertainties in the wave climate in the binning process (as discussed before) the effect is not expected to be significant.

8 Conclusion

The coastward channel slope of tidal channel Oostgat is eroding. The aim of this study is to increase our understanding of the coastal erosion processes. A detailed model has been created to simulate the flow and sediment transports in the tidal channel and surrounding area. This model is based on the existing Delft3D-NeVla model. The grid size has been refined around 4 times for both cell width and height. Furthermore, waves have been incorporated into the model using a representative wave climate. To reduce calculation time, the time series has been reduced to a morphological tide with a RMS value of 0.1 compared to sediment transports for two spring-neap cycles. The results of the new model show similar output to the calibrated Delft3D-NeVla model. In addition the model results show a divergence of transports along the coast between Zoutelande and Westkapelle which results in erosion. The new model can therefore be used for the modelling of the coastal erosion of tidal channel Oostgat.

Both waves and wind have a minor effect on the erosion at the channel wall. The limited effect of waves is possibly due to the orientation of the coast, which, for the dominant wave directions northwest and southwest, causes no transport since they are normal or parallel to the coast. Wind affects the upper part of the flow by adding additional shear stress. Due to the depth of the channel, the effect on the coastward erosion is limited. The tide is the main contributor to the coastward erosion near Zoutelande and is forced by a water level gradient between Vlissingen and Westkapelle. A transport gradient along the coast causes erosion over a long stretch of the channel wall from Zoutelande to Westkapelle.

There are three effects that increase ebb dominant transports at the coastward side of the channel between Westkapelle and Zoutelande. An onshore directed net discharge across the 'Bankje van Zoutelande' flows out of the channel in both northern and southern direction causing a divergence of flows in the channel. These flows cause an overall net transport in ebb-direction for the northern part of the channel and a flood-directed transport in the southern section.

There are also cross-channel differences in tide dominance. Due to the inertia of the flood tidal flow around the bend at Westkapelle and the decreasing channel depth towards the south, there is an offshore directed discharge during flood tide across the banks that causes a shift of the tidal flow magnitude in seaward direction from the channel axis. This causes a flood dominance and resulting transports along the 'Bankje van Zoutelande' in the Oostgat towards the south. The shift of the flood velocities away from the coast causes an ebb dominance on the coastward side of the channel between Westkapelle and Zoutelande with a resulting ebb directed sediment transport gradient along the channel wall.

Finally, the observations of ebb velocities also show a strong shift of the ebb velocities towards the coast which increases towards the bend at Westkapelle. This effect further increases the coastward ebb dominance. The acceleration of the coastward flow can have multiple causes that have not yet been confirmed. Further study using an idealized model is required to further narrow down the concepts that cause the coastal erosion.

9 Recommendations

The model that was used in this study contains a broad range of processes that all have effect on the flow velocities and transports. This makes it more difficult to narrow down the cause of certain flow or transport patterns. By simplifying the model and reducing the amount of processes included in the model, patterns can be more easily related to the cause. For further analysis of the erosion of the tidal channel, the transport gradient on the coastward side should be explained. Based on the results of this study I propose to further evaluate the effect of a significant bend in a tidal channel. Secondly, the effect of a local narrowing of a tidal channel on the coastward side should also be investigated. A third effect that should be analyzed with an idealized model is the divergence of the flow on the coastward side at the outflow of the channel. The results of this study suggest that tidal asymmetry in the Oostgat does not have a significant effect on the erosion. The tide can therefore be represented as a sinusoidal signal. Waves and wind have limited effect on the coastal erosion and can also be left out of the model. Since only one of the effects is related to the discharge across the banks, these can be left out of the model for a first attempt (Figure 9.1).

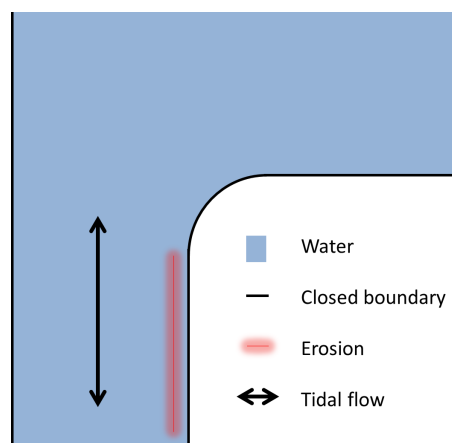


Figure 9.1: Model domain for the simplified model

A study into the impact of 3D flow effects is required to further support the results in this study. This process has not been included in the model and could potentially be important for the coastal erosion.

Future models of the tidal channel that aim at reproducing the coastward erosion of the channel slope only have to include the tide, since this is the main contributor to the erosion near Zoutelande. For modelling of the transport patterns around the 'Bankje van Zoutelande', Elleboog and Rassen, the waves and wind should be included. Waves and wind have the most significant effect in shallow areas and secondly, the transport direction across the banks is determined by the combination of all effects.

Based on the conceptual model, measures to reduce erosion could be derived. One of these scenarios is raising the bar between Oostgat and Sardijngeul, forcing the tide through Oost Deurloo. Since the flood tide carries sediment from Oostgat to Sardijngeul, this measure would cause sedimentation in the Oostgat and therefore strengthen the measure. The limited depth of Oost Deurloo could push the tide back into the Oostgat, reducing the effectiveness. Similar scenarios can be derived from the transport paths and descriptions that have resulted from this study.

10 References

- Cleveringa, J., 2008. *Morphodynamics of the Delta coast*. WL|Delft Hydraulics. 1, 7
- Deltares, 2013. *Delft3D Flow User Manual*, 3.15.30059 ed. 15, 43, 45
- Elias, E. P. L., P. L. Barnard and J. Brocatus, 2009. "Littoral transport rates in the Santa Barbara Littoral Cell; a process-based model analysis." *Journal of Coastal Research* Special Issue 56. 3
- Elias, E. P. L., G. Gelfenbaum and A. J. Van der Westhuysen, 2012. "Validation of a coupled wave-flow model in a high-energy setting: The mouth of the Columbia River." *Journal of Geophysical Research* 117. 2
- Erkens, G., 2003. *Analyse Multibeam data Oostgat*. Rijksinstituut voor Kust en Zee. 1, 7, 9, 10, 18, 33
- Grasmeijer, B., 2013. *Actualisatierapport Delft3D Schelde-estuarium*. Arcadis. 13
- Hordijk, D., 2002. *Geulwandsuppletie Oostgat westerschelde*. Delft University of Technology. 1, 7, 9, 10
- Kuijper, C., R. Steijn, D. Roelvink, T. Van Der Kaaij and P. Olijslagers, 2004. *Morphological modelling of the Western Scheldt*. Rijkswaterstaat. 5
- Lesser, G. R., J. A. Roelvink, J. A. T. M. Van Kester and G. S. Stelling, 2004. "Development and validation of a three-dimensional morphological model." *Coastal Engineering* 51: 883–915. 2
- Mol, A. C. S., 2007. *R&D Kustwaterbouw Reductie Golfbrandvoorwaarden*. 3, 15, 53
- Rijksoverheid Nederland, 2008. "Helpdesk water - Dijkkring." <http://www.helpdeskwater.nl/onderwerpen/waterveiligheid/beleid/management-0/overstromingslexicon/lexicon/dijkkring/>. 1, 5
- Rijkswaterstaat, 2013. *Rapport kustlijnkaarten 2014*. 1, 8
- Rocha, V. L., Mariana, H. Michallet, A. Silva, Paulo, T. Abreu and E. Barthelemy, 2013. "Non-linearities of short and long waves across the shoaling, surf and swash zones: large-scale physical model results." In *Coastal Dynamics 2013*, pages 1329 – 1340. France. 29
- Roelvink, J. A. and M. J. F. Stive, 1989. "Bar-Generating Cross-Shore Flow Mechanisms on a Beach." *Journal of Geophysical Research* 94 (C4): 4785–4800. 29
- Steijn, R. and A. Van der Spek, 2005. *Mogelijkheden voor geulwandversterking of verlegging Oostgat/Sardijngeul*. Alkyon. 1, 5, 6, 7, 8, 10
- Tonnon, P. K. and J. J. Van der Werf, 2014. *Geulopdringing Zuidwest Walcheren*. Deltares. v, 1, 2, 5, 7, 8, 9, 13, 16
- Tonnon, P. K., J. J. Van der Werf and J. Mulder, 2009. *Morfologische berekeningen MER zandmotor*. Deltares. 53, 55
- Van der Spek, A. and E. Elias, 2013. "The effects of nourishments on autonomous coastal behaviour." In *Coastal Dynamics 2013*. 9

- Van der Werf, J. J. and C. B. Brière, 2013. *The influence of morphology on tidal dynamics and sand transport in the Scheldt estuary*. Deltares. [45](#)
- Van Ormondt, M. and J. G. De Ronde, 2009. *Mogelijke effecten Geulwandsuppletie Oostgat op de drempel tussen het Oostgat en de Sardijngeul*. TechReport. [5](#), [9](#)
- Van Rijn, B. W. F., 2012. *Influence of wave climate schematisation on the simulated morphological development of the Western Scheldt entrance*. Arcadis and Delft University. [15](#), [35](#), [53](#), [54](#)
- Vermaas, T. and A. Bruens, 2013. *Beheerbibliotheek Walcheren*. Deltares. [1](#), [2](#), [8](#), [9](#)
- Walstra, D. J. R., 2005. *Haalbaarheidsstudie Geulwandsuppletie Oostgat*. WL|Delft Hydraulics. [1](#), [5](#), [6](#), [8](#)

A What are the assumptions and equations Delft3D uses?

The manual summarizes the model as follows:

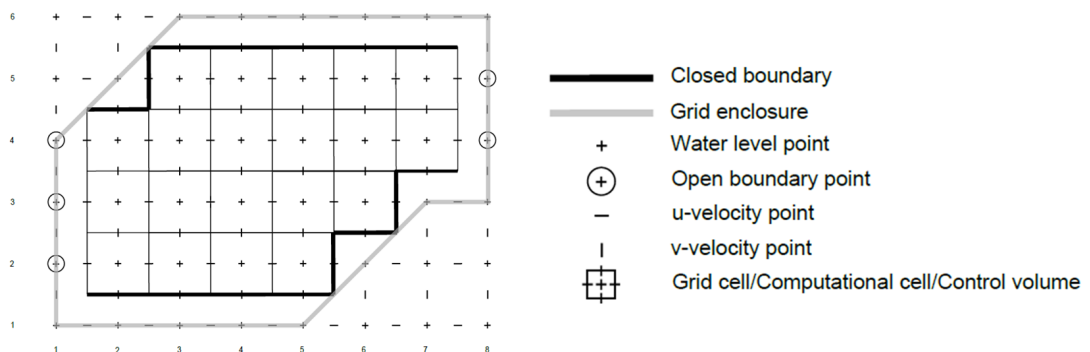
Delft3D-FLOW is a multi-dimensional (2D or 3D) hydrodynamic (and transport) simulation program which calculates non-steady flow and transport phenomena that result from tidal and meteorological forcing on a rectilinear or a curvilinear, boundary fitted grid. In 3D simulations, the vertical grid is defined following the sigma co-ordinate approach. (Deltares, 2013)

A.1 Grid

Delft3D uses finite differences to calculate the different processes. These finite differences are distributed differently for the horizontal and vertical plane. The calculations are performed with a staggered grid on the horizontal plain as displayed in Figure A.1

A.1.1 Horizontal staggered grid

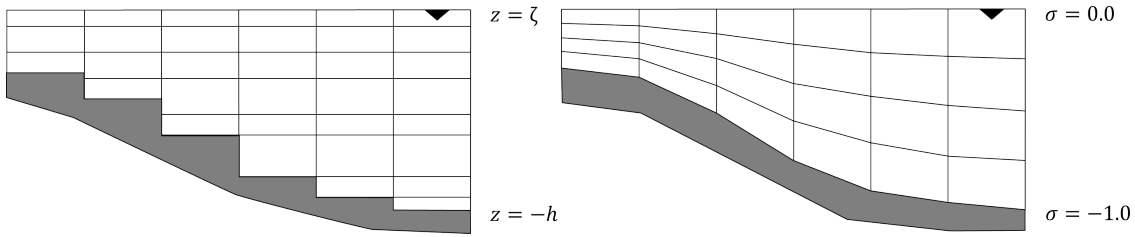
Figure A.1: Staggered grid with boundaries



A.1.2 Vertical σ -grid

For the cells in vertical direction a σ -grid is used which is displayed in Figure A.2. This grid type creates layers of cells where the height is scaled to the water depth. The cell density is higher for shallow water which enables more accurate calculations for shallow water. Furthermore the relative thickness of the layers does not have to be uniform. A higher layer density can be applied at the surface (wind and heat transfer) and at the bottom (sediment transport). The transformation to the σ -grid system is shown in Equation A.1.

$$\sigma = \frac{z - \theta}{d + \theta} = \frac{z - \theta}{H} \quad (\text{A.1})$$

Figure A.2: Vertical Z-grid and σ -grid

A.2 Hydrodynamic equations

Delft3D FLOW uses the Navier Stokes equation (A.2) which is derived from the law of preservation of impulse.

$$\rho \frac{d\mathbf{v}}{dt} = -\nabla \cdot \mathbb{P} + \mathbf{f} \quad (\text{A.2})$$

With \mathbf{v} the velocity of the fluid, ρ the density of the fluid, \mathbf{f} the force vector per volume, \mathbb{P} a tensor for the stress (viscosity, shear stress). Different assumptions that are made include incompressible fluid, shallow water conditions (Depth scale \ll Length scale) and an eddy viscosity for small-scale turbulence effects. The basic equations for horizontal momentum derived from the Navier Stokes equations written in terms of the velocity (assuming shallow water) are:

$$\frac{\partial U}{\partial t} + U \frac{\partial U}{\partial x} + V \frac{\partial U}{\partial y} + \frac{\omega}{h} \frac{\partial U}{\partial \sigma} - fV = -\frac{1}{\rho_0} P_x + F_x + M_x + \frac{1}{h} \frac{\partial}{\partial \sigma} \left(v_V \frac{\partial u}{\partial \sigma} \right) \quad (\text{A.3})$$

$$\frac{\partial V}{\partial t} + U \frac{\partial V}{\partial x} + V \frac{\partial V}{\partial y} + \frac{\omega}{h} \frac{\partial V}{\partial \sigma} - fU = -\frac{1}{\rho_0} P_y + F_y + M_y + \frac{1}{h} \frac{\partial}{\partial \sigma} \left(v_V \frac{\partial v}{\partial \sigma} \right) \quad (\text{A.4})$$

with U and V the depth averaged velocities in x and y direction respectively. f is the Coriolis parameter, g the gravitational acceleration and h the depth and v_V the vertical eddy viscosity. Pressure is included with P_x and P_y for which a Boussinesq approximation is applied. An unbalance in vertical momentum due to turbulence is added (M_x , M_y) and finally there is a radiation stress gradient (F_x , F_y). The vertical momentum equation combined with the shallow water assumption is reduced to a hydrostatic pressure (Equation A.5). Buoyancy effects and sudden variations in bed topography are not taken into account.

$$\frac{\partial P}{\partial \sigma} = -\rho g h \quad (\text{A.5})$$

The depth averaged for incompressible fluids over total depth is given by:

$$\frac{\partial \zeta}{\partial t} + \frac{\partial [h\bar{U}]}{\partial x} + \frac{\partial [h\bar{V}]}{\partial y} = S \quad (\text{A.6})$$

with ζ the surface elevation, h the water depth, \bar{U} and \bar{V} the depth averaged velocity vectors and S the source and sink term (discharge, withdrawal, precipitation and evaporation). The turbulence consists of a horizontal and vertical component. Of these, the horizontal component is much larger ($v_H \gg v_V$). This horizontal component consists of three parts. The first is the sub-

grid scale turbulence viscosity and represents eddies that are smaller than the grid resolution. The second component is the three-dimensional turbulence as is modeled by a 3D-turbulence closure model and the final part is the background viscosity in horizontal direction which must be defined.

A.3 Sediment transport

Based on the results from the hydrodynamics the transport rates are modeled with an advection-diffusion equation in three dimensions. The resulting changes to the bed bathymetry are calculated. A further explanation of the methods for calculating sediment transport can be found in the manual for Delft3D-Flow ([Deltares, 2013](#)).

A.4 Existing model

There is an existing model for the entire Western Scheldt area. This is a Delft3D model based on a previous model called NeVla ([Van der Werf and Brière, 2013](#)). The most important processes for this model are listed below including the implementations:

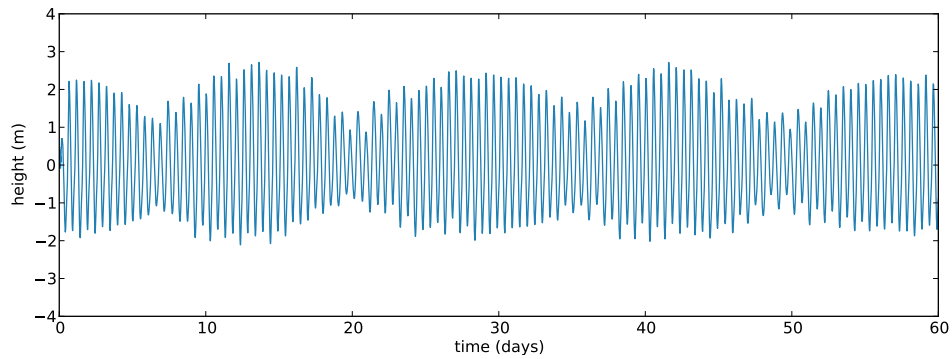
Tide	Included in the boundary conditions
Wind	Included as time series of velocities and directions at Vlissingen and implemented as uniform wind velocity field, which forces the water with a stress at the surface.
Waves	Not included in Delft3D-NeVla model
River discharges	Discharges for the different inflows at Zenne, Dijle, Grote Nete, Kleine Nete, Schelde, Dender, Bath and Terneuzen are included as time series.
Bed composition	The varying bed composition in the channel is included in the model. The depth of the sediment layer at locations with a hard clay layer is set to 0 which means no erosion will occur at these locations. This is a simplification of the real situation where this layer can erode but at a slower rate.

The curvilinear grid is refined locally at important locations which are mainly in the Scheldt estuary. The size of the grid cells near the Oostgat is coarser with cells of around 65m in longshore direction and 165m in cross shore direction. The initial bathymetry around the Oostgat contains data from 2011. The initial water level is set at 0m. By letting the model balance during the first period an equilibrium is expected to be reached from which the model can continue with the actual calculations. It is also possible to define a restart file which contains water levels from the end of another run that can be used as initial levels for the current run. The tide is included with different boundary conditions at the open boundaries. The cross shore boundaries are defined using a time series of current velocities. The boundary parallel to the shoreline is set to a Riemann condition. The Delft3D-NeVla model has been calibrated and validated based on water levels, discharges and current velocities ([Van der Werf and Brière, 2013](#)).

B Representative morphological tide

One of the most important forcing mechanisms that influence the erosion of the channel slope at the Oostgat is the tide. Since a detailed analysis of one or more spring neap cycles is computationally intensive the time span of the model should be reduced. However, the most important tidal effects should still be present in the model. By identifying a representative morphological tide the simulation only has to run for one (or possibly two M2 cycles. The transport over this morphological tide should have the same or a similar average as the entire spring neap cycle. Reducing the tide to a representative tide is done by analysing the difference between the residual transports for the M2 cycles averaged over the spring neap cycle to the residual transport for every M2 cycle. Before this analysis can be done, the tidal data has to be divided into spring neap cycles and M2 tides. This decomposition is based on the water level (Figure B.1).

Figure B.1: Water level elevations over time at tidal channel Oostgat



The M2 tides can be selected by splitting at every second 0-crossing in the water level time series. Since the daily inequality is also clearly visible in the time series the representative tide is also calculated using two M2 periods (every fourth 0-crossing of the water level). The quality of the results can be compared and a decision can be made which representative tide will be used in the model. Dividing the time series in spring neap cycles is done by identifying the M2 and S2 frequencies using a Fourier transformation (Figure B.2). From these frequencies the spring neap period can be calculated using:

$$T_{cycle} = \frac{1}{f_{S2} - f_{M2}} = 14.22 \text{ days} \quad (\text{B.1})$$

with T_{cycle} the period of the spring neap cycle and f the frequency of a tidal component.

Since the first 30 days are estimated to be affected by the balancing of the model the second half of the time series is used for further analysis of transports. From this period of 30 days two spring neap cycles containing an integer number of tidal cycles are selected (Figure B.3). The splitting of M2 tides results in 60 cycles. Due to the importance of the daily inequality also pairs of two M2 tides are selected. Since the tides can be combined in two different ways (also with an offset of 1 cycle) this results in another 60 cycles.

The next step is to estimate the quality of each tidal cycle. The reference value is based on the average residual transport per tide over the entire spring neap cycle. At locations with low

Figure B.2: Fourier transformation of water level elevations with tidal components M2 and S2

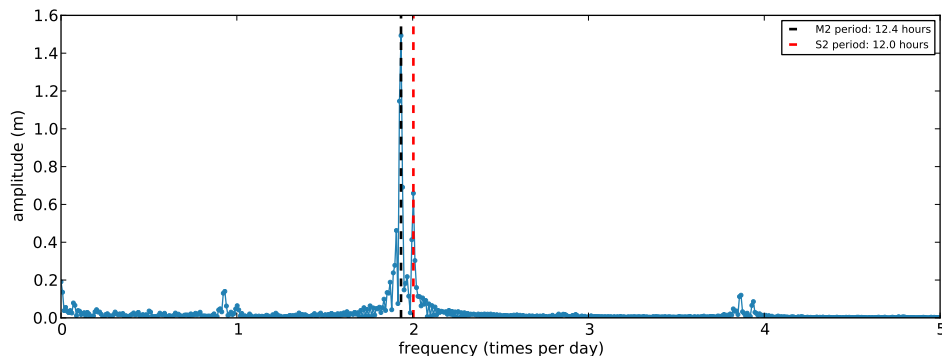
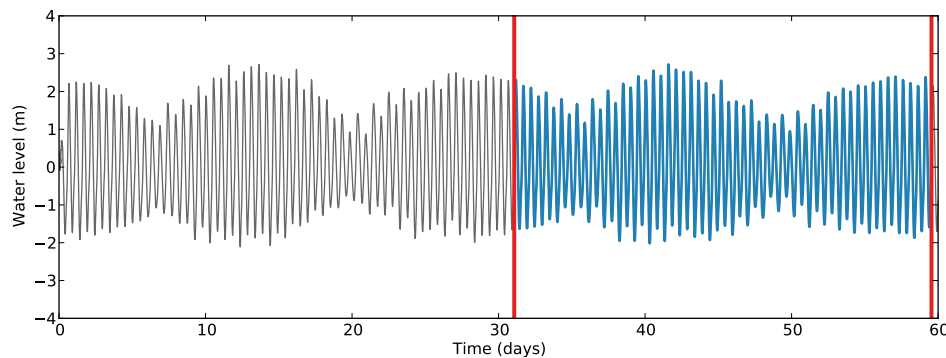


Figure B.3: Spring neap cycle domain as used for the derivation of the morphological tide



transport the difference to the average is also important, because for this study we are interested in detailed residual sediment transport paths for which the small transports can play an important role as well. This means the deviation from the average must be normalized. However, the transport time series has an alternating pattern with an average near 0. This can therefore not be used for scaling of the transports. By taking the absolute value of the transport time series and then averaging, the resulting value has the same order of magnitude as the transports and can be used for normalizing the transport deviations.

The average residual transports over the two spring neap cycles are calculated using:

$$Q_{s;res,avg} = \frac{1}{n_c} \sum_{t=0}^{2T_{sn}} q_s \quad (\text{B.2})$$

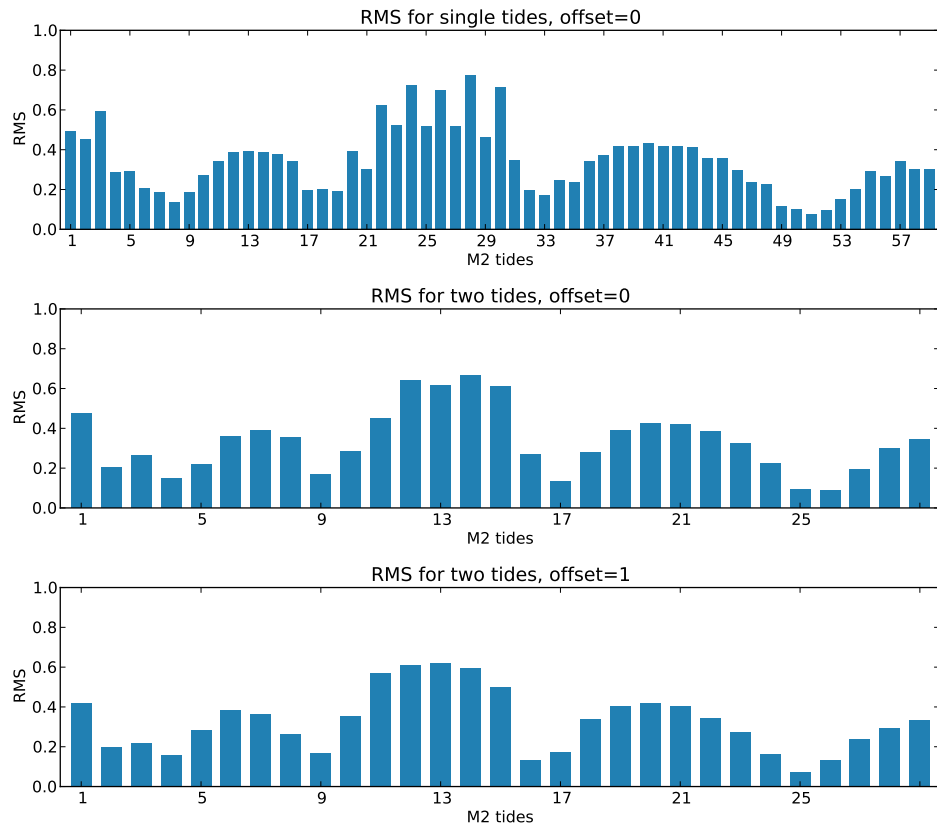
with q_s the sediment transport at each time step, T_{sn} the period of a spring neap cycle and n_{M2} the number of tidal cycles in this period. Normalizing of the transports is done using the absolute transport values:

$$Q_{s;scale} = \frac{1}{n_c} \sum_{t=0}^{2T_{sn}} |q_s| \quad (\text{B.3})$$

A Root Mean Square is applied to the results to estimate the best representative morphological tide. This is done using the following formula:

with $Q_{s,res,avg;i}$ the average residual transports for a cross section i , $Q_{s,res;i,j}$ the residual transport at a cross section of a tide j and $Q_{s,scal;i}$ the scaling value of a cross section. The results of the Root Mean Square are shown in Figure B.4.

Figure B.4: Root Mean Square of normalized deviations



The single tide with the lowest RMS is number 51. The best pair without offset is 26 and with offset 25 is the best. The deviation from the average of residual tidal transports is shown in figures B.5, B.6 and B.7 (cross sections numbered from north to south). From these tides the best representative tide has to be selected. This is based on three main criteria:

- ◇ Similarity in scale: is the amount of tidal transport similar to the averaged transport?
- ◇ Similarity in direction: is the direction of tidal transport the same as the averaged transport?
- ◇ Location of large deviations: are the largest deviations in or near the study area?

Before looking at the deviations the area of interest has to be defined. Since we are interested in transports in the Oostgat these cross sections are obviously important. Furthermore the transports near the 'Bankje van Zoutelande' might have an important role due to the migration of the offshore banks and other cross shore transport as is also mentioned in the hypotheses. The single tide (Figure B.5) shows a good similarity in scale. The relative differences are mostly small. There are three important peaks at the Bankje van Zoutelande (north side), Oostgat (near Zoutelande) and Sardijnegeul. The directions are, except for the Sardijnegeul, in the right direction.

The peaks at the 'Bankje van Zoutelande' and Oostgat are peaks within the study area that show deviations of more than a factor 4. An analysis of tidal flows at these locations for this tide can therefore deviate from the average tidal flows. The pair of tides with no offset (Figure B.6) also has a large peak at the north side of the Bankje van Zoutelande which deviates strongly from the average. There is another peak at the Oostgat near Zoutelande which is similar in size compared to the previous representative tide. All cross sections have transports in the right direction. The large peak at the 'Bankje van Zoutelande' is inside the study area and could therefore give unwanted deviations in the results. The final pair of tides (Figure B.7) that has an offset of 1 has a large peak at the Oostgat near Zoutelande which is larger than the other representative waves. There is also a peak of significant height at the Sardijngemaal. The transport direction at Oostgat 8 is reversed. This last deviation gives reversed transport directions at the most important location inside the study area and a large overestimation just south of this point and is therefore not useful as a representative tide. The single tide is the best tide for a representative tide since it describes the transport direction inside the study area correctly as well as the scale for most of the locations.

Figure B.5: Deviations from mean transport of best representative single tidal cycle

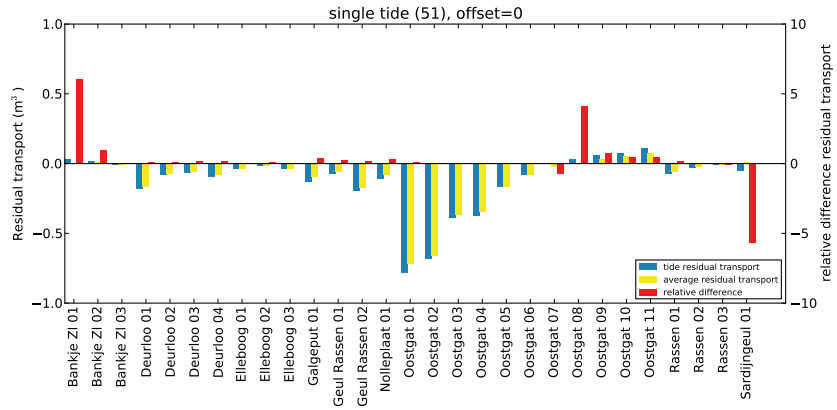


Figure B.6: Deviations from mean transport of best representative pair of tidal cycles with no offset

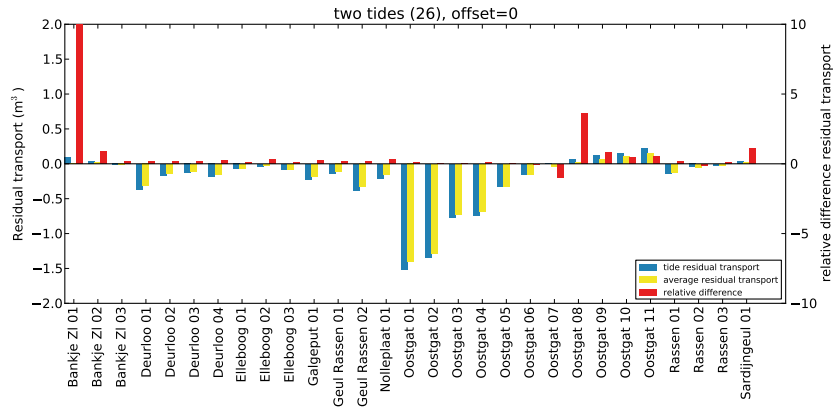
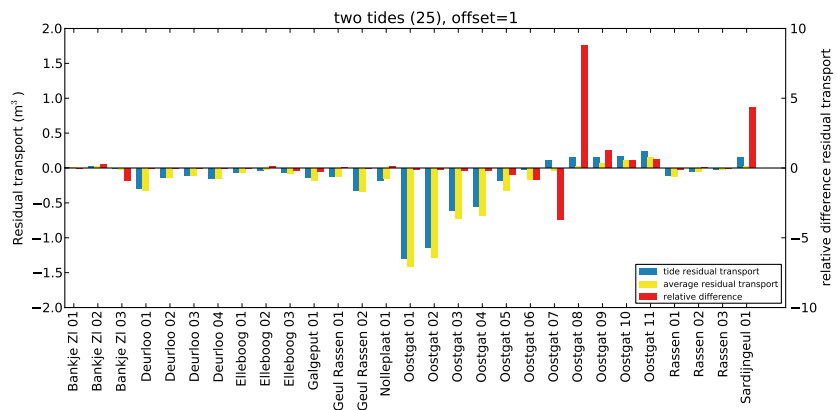


Figure B.7: Deviations from mean transport of best representative pair of tidal cycles with offset of 1



C Representative wave climate

A representative wave climate has been derived for the Western Scheldt by [Van Rijn \(2012\)](#). Wave heights measured at the buoy at Schouwenbank were used (1981-2001) in combination with wave directions at Euro Platform. Wind data averaged per day was used from measurements at Vlissingen. The waves were binned into 12 direction classes and 6 velocity classes. This resulted in 72 wave classes of which 18 classes did not occur. The remaining 54 wave classes with each a chance of occurrence were simulated. Out of all these classes a limited number of wave conditions is selected that best represent the morphological change in the model area. This selection procedure is done using the Opti method ([Mol, 2007](#)) as was also used by [Van Rijn](#). Another example of deriving a representative wave climate using the Opti method can be found in [Tonnon et al. \(2009\)](#).

C.1 Approach

For this study the 54 wave classes (Table C.1) are used to derive a representative wave climate for the Oostgat tidal channel. These wave classes are simulated in Delft3D and based on the results the representative wave classes are selected using the Opti method. The mean total transport at the Oostgat, Bankje van Zoutelande and Deurloo Oost is used as a criterion for reducing the number of wave conditions. The Opti method output is a stepwise reduction of wave conditions with related relative weighted RMS. The aim is to have around 8 wave conditions that represent the entire wave climate. A different number of conditions can be considered if this results in a significant improvement of the quality of the results.

#	Waves				Wind			Weight (%)
	Height (m)	Period (s)	Direction (°)	Speed (m/s)	Surge height (m)	Speed (m/s)	Direction (°)	
1	0.49	5.28	15.85	16.00	-0.10	3.04	110.67	2.722
2	0.54	5.42	0.81	8.00	-0.06	2.95	49.45	2.490
3	0.55	5.41	9.64	12.00	-0.09	2.97	79.79	2.409
4	1.01	5.37	23.12	9.00	-0.10	6.46	49.20	3.924
5	1.07	5.48	7.45	5.00	-0.03	6.52	21.24	4.307
6	2.07	6.54	9.21	6.00	0.00	10.21	21.54	0.902
7	0.74	4.74	76.64	17.00	-0.19	6.31	109.55	3.104
8	0.93	5.24	41.01	13.00	-0.17	6.37	79.90	3.581
9	1.78	6.12	49.22	14.00	-0.38	10.39	80.25	0.741
10	2.10	6.58	26.60	10.00	-0.18	10.53	49.44	0.799
11	2.66	6.85	42.25	15.00	-0.43	14.00	74.29	0.012
12	3.25	7.72	24.73	11.00	-0.35	14.48	50.00	0.067
13	0.61	4.51	139.25	21.00	-0.13	6.14	140.12	2.349
14	0.75	4.72	201.30	24.00	-0.08	6.35	172.05	3.338
15	1.21	5.02	158.75	22.00	-0.21	10.15	142.17	0.197
16	1.46	5.50	87.51	18.00	-0.43	10.27	106.35	0.323
17	1.47	5.47	197.67	25.00	-0.19	10.27	174.33	0.719
18	2.29	6.42	78.60	19.00	-0.77	14.22	100.00	0.009
19	0.92	5.00	223.91	28.00	-0.03	6.73	200.52	5.796
20	1.72	5.92	219.23	29.00	-0.03	10.56	201.69	3.258
21	2.41	6.54	203.63	26.00	-0.40	14.35	178.13	0.027

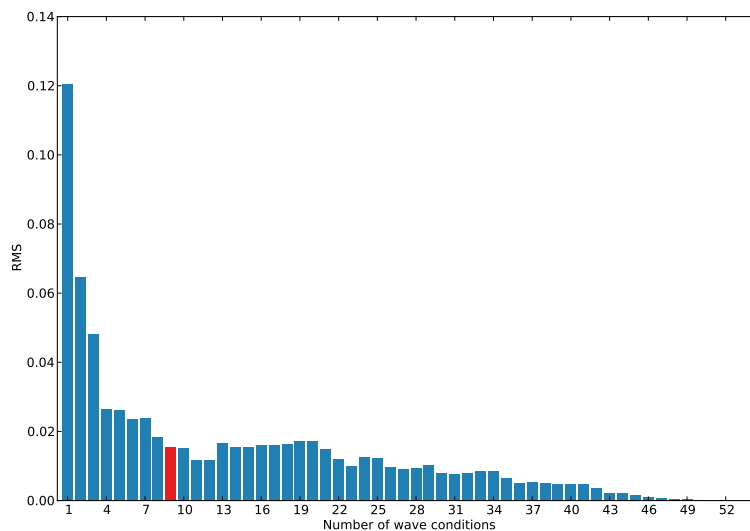
#	Waves				Wind			Weight (%)
	Height (m)	Period (s)	Direction (°)	Speed (m/s)	Surge height (m)	Speed (m/s)	Direction (°)	
22	2.71	6.97	221.76	30.00	-0.08	14.79	203.74	0.279
23	3.77	7.63	205.05	31.00	-0.22	18.97	206.67	0.005
24	3.78	7.93	223.97	41.00	0.78	18.90	258.00	0.009
25	0.99	5.18	242.37	33.00	0.03	6.79	230.76	7.065
26	1.88	6.22	231.46	34.00	0.10	10.71	231.36	5.031
27	2.90	7.27	229.60	35.00	0.16	14.70	231.94	0.548
28	3.26	7.85	247.17	40.00	0.47	15.03	259.31	0.346
29	3.89	8.22	227.41	36.00	0.22	19.01	233.33	0.026
30	5.05	9.36	249.00	42.00	1.06	23.40	260.00	0.002
31	0.48	5.19	270.19	23.00	-0.06	3.03	170.35	2.402
32	0.51	5.23	277.25	27.00	-0.04	3.00	199.89	2.752
33	1.07	5.36	262.01	38.00	0.08	6.69	258.22	5.806
34	2.04	6.47	249.69	39.00	0.23	10.62	258.14	2.793
35	3.53	8.07	273.98	46.00	0.78	14.84	288.22	0.366
36	4.50	8.78	268.50	47.00	0.87	18.75	281.25	0.014
37	0.54	5.23	283.95	32.00	-0.02	3.04	230.29	3.020
38	0.60	5.34	297.10	37.00	0.01	3.07	259.32	2.659
39	1.28	5.75	295.03	44.00	0.15	6.72	289.09	3.530
40	2.38	6.95	285.37	45.00	0.42	10.78	289.03	2.074
41	3.78	8.48	313.84	51.00	0.87	14.65	316.43	0.168
42	5.16	9.62	308.93	52.00	1.43	19.38	320.00	0.005
43	0.67	5.51	313.99	43.00	0.01	2.93	289.65	2.281
44	0.68	5.58	329.39	48.00	0.00	2.95	319.78	2.250
45	1.35	5.97	325.46	49.00	0.16	6.74	320.01	2.726
46	2.45	7.11	321.08	50.00	0.43	10.67	319.27	1.131
47	3.90	8.58	335.62	56.00	0.77	14.74	348.64	0.075
48	4.85	10.27	339.00	57.00	1.15	18.13	340.00	0.002
49	0.46	5.23	352.85	20.00	-0.08	3.01	139.53	2.481
50	0.61	5.55	353.60	4.00	-0.04	3.01	20.32	2.654
51	0.66	5.63	344.11	53.00	-0.02	2.96	350.09	2.360
52	1.31	5.92	346.50	54.00	0.07	6.64	350.09	3.078
53	2.48	7.17	344.09	55.00	0.30	10.56	349.61	0.960
54	3.86	8.33	356.72	7.00	0.26	14.41	16.47	0.029

Table C.1: Wave classes based on measurements at Schouwenbank / Euro Platform binned by direction and wave height (Van Rijn, 2012)

C.2 Results

In figure C.1 the RMS error for every set of representative wave conditions is shown. For a lower number of representative conditions the error is larger, since a larger part of the actual climate has been left out. There are some fluctuations in the error which can be explained by the optimization approach of OPTI which uses a random selection in combination with an optimization approach. The random effect can be reduced by increasing the number of iterations. For this analysis 1000 iterations have been performed as was also done for a study by [Tonnon *et al.* \(2009\)](#).

Figure C.1: Relative weighted root mean square error for representative wave climate for different amounts of wave conditions with the selected choice of 9 wave conditions with relative weighted RMS of 0.0156



The number of wave conditions for the representative wave climate should be a balance between accuracy and calculation time. Based on the RMS errors and the feasibility of the number of calculations, a set of 9 wave conditions has been selected with a RMS error of 0.0156.

The conditions that were selected from the wave climate are shown in table C.2.

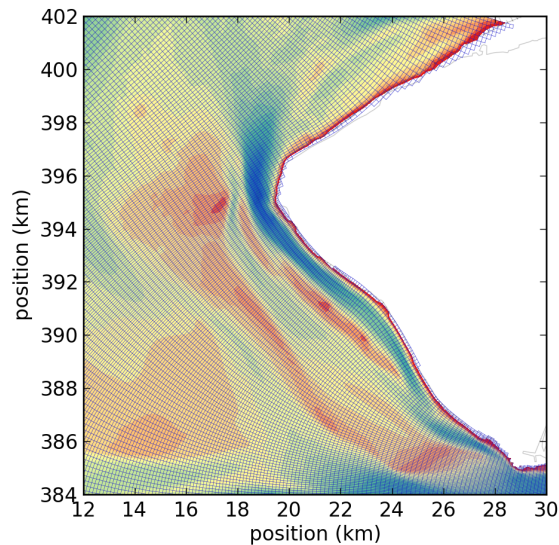
#	Weight [-]	Height (m)	Direction (°)
3	.0683	0.55	9.64
5	.2270	1.07	7.45
14	.4125	0.75	201.30
19	.0076	0.92	223.91
26	.1581	1.88	231.46
33	.0287	1.07	262.01
40	.0467	2.38	285.37
45	.0268	1.35	325.46
52	.0262	1.31	356.72

Table C.2: Representative wave conditions

D Grid design

The existing grid in the Delft3D-NeVla model has a grid of 3000 by 379 cells of which 240.903 cells are active calculation cells. At the Oostgat tidal channel the grid has cells of 60m in long-shore and 160m in cross shore direction (Figure D.1). Further into the Western Scheldt the cell size is more detailed which also indicates that the focus of the existing model is not the Oostgat but the Western Scheldt estuary. In addition the grid does not smoothly follow the coastline. Some cells have been cut away to create the strongly curved coastline.

Figure D.1: Existing Delft3D-NeVla grid with cells of 160 by 60m at the Oostgat tidal channel



Since this study focuses on the Oostgat and detailed results can be of major importance, it is useful to adjust the calculation grid. For this adjustment the following improvements can be made:

- ◇ Cell size in the channel can be refined.
- ◇ The grid can follow the local bathymetry. Following the bed forms and flow patterns can increase the quality of the results in Delft3D. Also the defining of cross sections is easier since they can follow the straight grid lines.
- ◇ The rough edges can be made smooth by curving the grid along the coast. If possible this includes the curve at the head of Walcheren.

First the area of interest is defined where the grid has to have the most detail. Next the approach of creating the grid and deriving boundary conditions for this new grid is described. The quality of the grid is discussed based on criteria from the Delft3D flow manual and finally the results for the nested model are compared to the coarser model.

D.1 Area of interest

The focus of the research is the landward directed channel slope of the tidal channel Oostgat. Mechanisms that determine the migration behaviour of the channel are investigated. These processes can be influenced by local morphological elements. At least the following morphological elements should be included in the model and have comparable results to the coarse model:

- ◇ Oostgat
- ◇ Bankje van Zoutelande
- ◇ Geul van de Rassen/Oost Deurloo

D.2 Approach

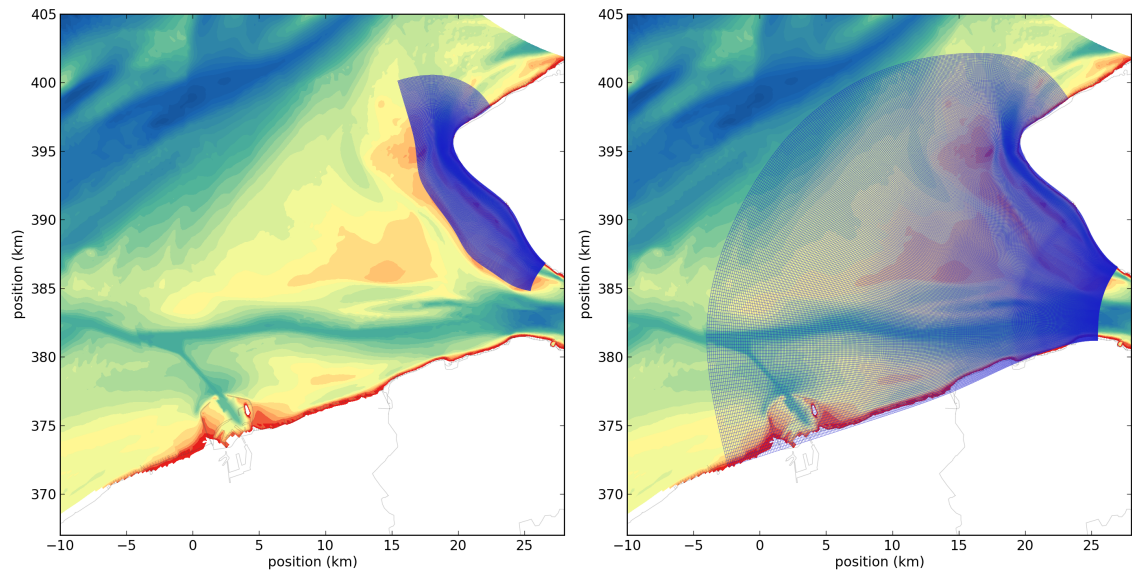
First a new grid has to be created. Using RGFGRID the system boundaries are set using splines. Within these boundaries multiple splines are placed to determine the grid line spacing and cell orientation. Based on this spline structure the cells are interpolated. The grid is refined at the coastward side of the tidal channel Oostgat. Coarser grid cells are applied further away from this area to reduce calculation time. The grid properties are evaluated and adjustments are made to comply with the maximum values as mentioned in the Delft3D flow manual:

- ◇ M-smoothness (<1.2)
- ◇ N-smoothness (<1.2)
- ◇ Aspect ratio (<2 or possibly higher in areas where the main flows are in the direction of the grid lines)
- ◇ Orthogonality (<0.02)

Next the new boundary conditions have to be derived from the coarse model using the nesting procedure. The Delft3D nesting procedure consists of three steps. First observation points are added to the coarse model at both ends of each open boundary section in the refined grid. A set of 4 observation points is used per location with a weight for each point based on the distance from the boundary to smooth local irregularities. Enough boundary sections have to be defined to capture variations along the boundary since the values between boundary section ends are interpolated. The second step is to run the coarse model with the defined observation points to generate a time series for each observation point which includes all relevant parameters that should be transferred to the finer grid. The last step is to generate a time series for each cell at the boundary in the fine model based on the calculated time series at the observation points. The boundary type can be set to one of these:

- ◇ Water level
- ◇ Flow velocities
- ◇ Neumann (water level gradient)
- ◇ Riemann (flow velocity combined with wave celerity)
- ◇ Discharge

Figure D.2: Grid designs



(a) First attempt with only area of interest
(578x122 cells; resolution Oostgat 15x25m)

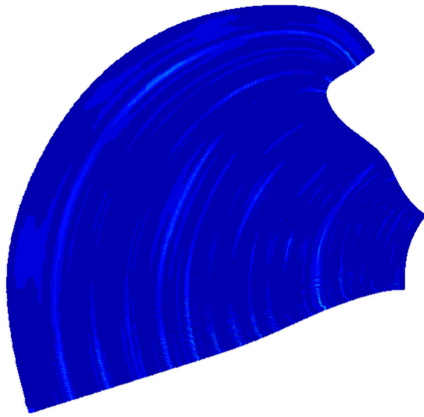
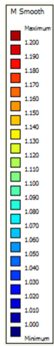
(b) Second attempt with entire outer delta
(506x322 cells; resolution Oostgat 25x25m)

A disadvantage of the Delft3D model is that boundaries in the model can only have a single time series defined. This means it is not possible to define a vector value since this requires two components (either X and Y, M and N or direction and magnitude). Only the vector magnitude orthogonal to the boundary is given. However, the tidal flow direction at the north and west boundary rotates over a tidal cycle. This rotation can therefore not be nested to the finer grid using a vector based boundary condition. Only water level boundaries are directionless and can therefore be applied at this boundary. The flow direction at the mouth of the Western Scheldt can be schematized as a vector with fixed direction. Flow velocities are therefore used at this boundary to also capture the Scheldt discharge in the model.

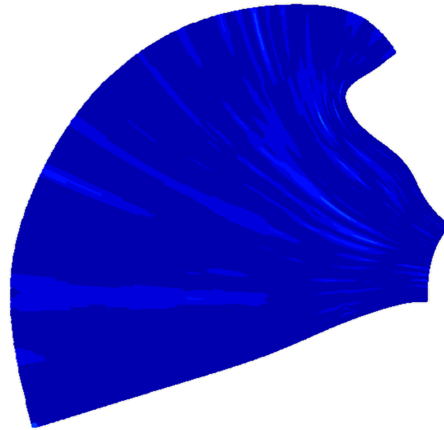
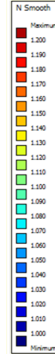
D.3 Grid quality

The first attempt for a grid design (Figure D.2a) included only the area of interest but was unable to reproduce the flow velocities at the western boundary. This was probably due to the complex flows around the boundary that are not represented by only the water level that is applied at the boundary.

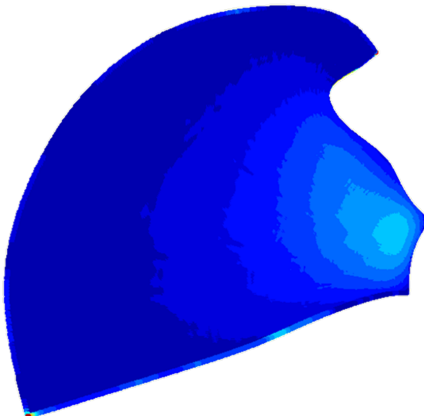
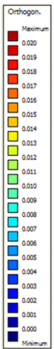
To improve the quality of the model the domain was increased to contain the entire outer delta of the Western Scheldt estuary. The boundary at the Western Scheldt was set to flow velocities since in the previous attempt these were able to reasonably approach the flow velocities in the coarse model. The open boundary at the sea side was set to water levels. The resulting grid is shown in Figure D.2b. Based on the criteria as defined in the manual the grid has been evaluated. The results for the criteria are shown in Figures D.3a, D.3b, D.4a and D.4b. The colour scale has been set between the minimum possible value and the maximum allowed value. Only the orthogonality exceeds the allowed value but this is limited to two cells at the corner of the grid. This is not near the area of interest. All other parameters comply with the given conditions. The resolution at the Oostgat is around 25 by 25m. To the south near the Sardijngeul the grid size is very fine due to the narrowing of the grid domain at this location. The grid contains a total of



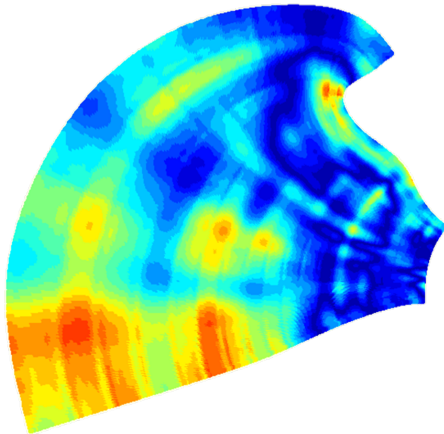
(a) *M-Smoothness*
(plot range 1.0-1.2; max 1.06)



(b) *N-Smoothness*
(plot range 1.0-1.2; max 1.04)



(a) *Orthogonality*
(plot range 0.00-0.02; max 0.028)



(b) *Aspect ratio*
(plot range 1.0-2.0; max 1.87)

about 170.000 cells. This is about 1.5 times less than the original model.

D.4 Comparison of model results

The results for the new and more detailed grid should be similar to the coarse grid. The differences between the coarse and fine grid can be a result of unwanted deviations in the fine grid caused by inaccuracies in reproducing the coarse grid results. Another possibility is that the fine grid is actually producing better results. The more detailed grid is able to simulate complex flows in more detail. It is difficult to differentiate between these two sources of inaccuracy.

The comparison between the coarse and fine grid is shown in figures D.5, D.6 and D.7. The comparison is made for water level, flow velocities and sediment transport (suspended and bed load). They are expected to have increasing deviations, because the water level forces the flow velocities (surface level gradient) and the flow forces the sediment transports exponentially. Deviations therefore build up.

The water levels and flow velocities are very similar for all three observation points. The deviations are mainly differences in scale; the shape of the graphs is similar for the coarse and fine grid. Oostgat 5 shows very similar results whereas Oostgat 1 has larger deviations of up to twice the transport rates.

Figure D.5: Comparison for observation point Oostgat 1

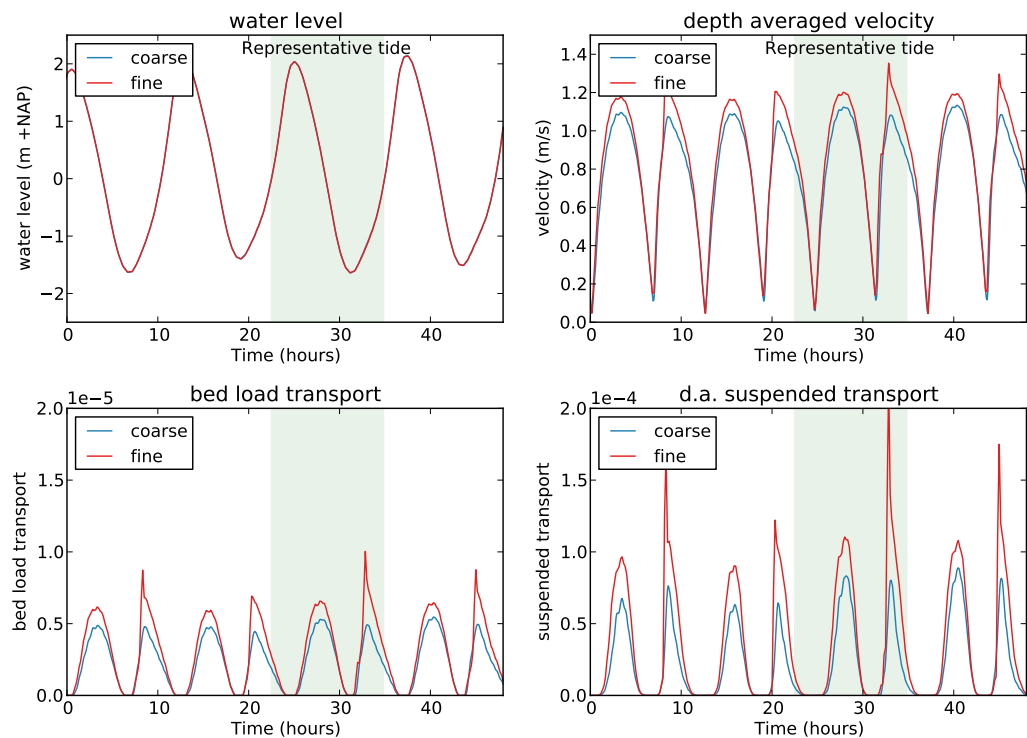


Figure D.6: Comparison for observation point Oostgat 5

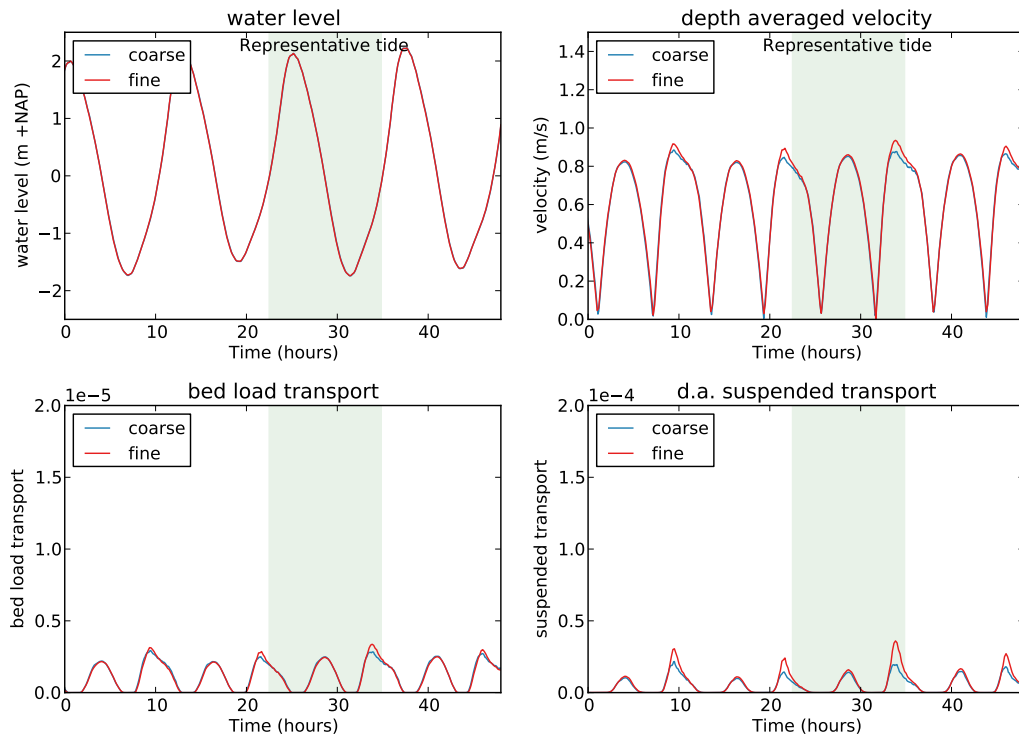
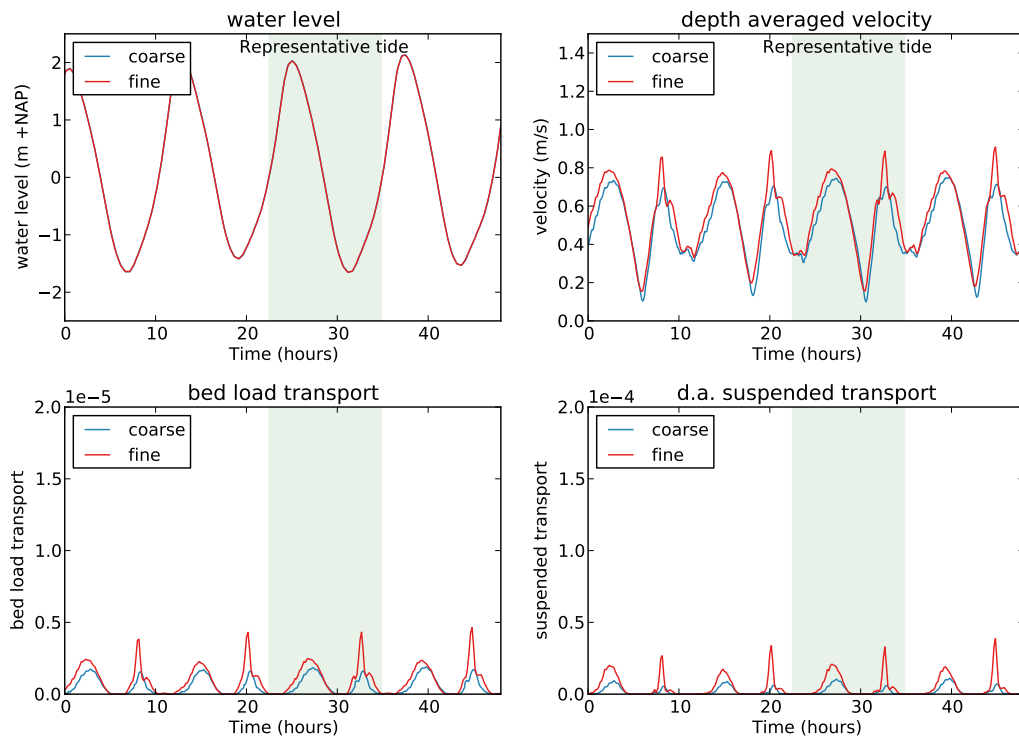


Figure D.7: Comparison for observation point Bankje van Zoutelande 1



E Derivation of velocity driven transport components

$$\mathbf{q} = \alpha \mathbf{v} |\mathbf{v}|^2 \quad (\text{E.1})$$

In order to evaluate the different contributions of transport by residual flow, transport due to velocity skewness and multiple interaction effects is investigated. The velocities are divided in an average or residual component and a time varying component with an average of zero (see equation E.2).

$$\mathbf{v}(t) = \bar{\mathbf{v}} + \tilde{\mathbf{v}}(t) \quad (\text{E.2})$$

$$q_x = \alpha \left((\bar{v}_x + \tilde{v}_x)^2 + (\bar{v}_y + \tilde{v}_y)^2 \right) (\bar{v}_x + \tilde{v}_x) \quad (\text{E.3})$$

$$\begin{aligned} \frac{q_x}{\alpha} = & \bar{v}_x (\bar{v}_x^2 + 2\bar{v}_x \tilde{v}_x + \tilde{v}_x^2 + \bar{v}_y^2 + 2\bar{v}_y \tilde{v}_y + \tilde{v}_y^2) + \\ & \tilde{v}_x (\bar{v}_x^2 + 2\bar{v}_x \tilde{v}_x + \tilde{v}_x^2 + \bar{v}_y^2 + 2\bar{v}_y \tilde{v}_y + \tilde{v}_y^2) \end{aligned} \quad (\text{E.4})$$

$$\begin{aligned} \frac{q_x}{\alpha} = & \bar{v}_x (\bar{v}_x^2 + \bar{v}_y^2) + \bar{v}_x (\tilde{v}_x^2 + \tilde{v}_y^2) + \\ & \tilde{v}_x (\bar{v}_x^2 + \bar{v}_y^2) + \tilde{v}_x (\tilde{v}_y^2 + \tilde{v}_x^2) + \\ & 2\bar{v}_x (\bar{v}_x \tilde{v}_x + \bar{v}_y \tilde{v}_y) + 2\tilde{v}_x (\bar{v}_x \tilde{v}_x + \bar{v}_y \tilde{v}_y) \end{aligned} \quad (\text{E.5})$$

$$\frac{\langle q_x \rangle}{\alpha} = \bar{v}_x (\bar{v}_x^2 + \bar{v}_y^2) + \bar{v}_x \langle \tilde{v}_x^2 + \tilde{v}_y^2 \rangle + \langle \tilde{v}_x (\tilde{v}_y^2 + \tilde{v}_x^2) \rangle + \langle 2\tilde{v}_x (\bar{v}_x \tilde{v}_x + \bar{v}_y \tilde{v}_y) \rangle \quad (\text{E.6})$$

$$\frac{\langle \mathbf{q} \rangle}{\alpha} = \bar{\mathbf{v}} |\bar{\mathbf{v}}|^2 + \bar{\mathbf{v}} \langle |\tilde{\mathbf{v}}|^2 \rangle + \langle \tilde{\mathbf{v}} |\tilde{\mathbf{v}}|^2 \rangle + \langle 2\tilde{\mathbf{v}} (\bar{\mathbf{v}} \cdot \tilde{\mathbf{v}}) \rangle \quad (\text{E.7})$$